THE JOURNAL OF BIOLOGICAL CHEMISTRY VOL. 289, NO. 43, pp. 29767–29789, October 24, 2014
Published in the U.S.A.

Selective Impairment of a Subset of Ran-GTP-binding Domains of Ran-binding Protein 2 (Ranbp2) Suffices to Recapitulate the Degeneration of the Retinal Pigment Epithelium (RPE) Triggered by *Ranbp2* Ablation*[S]

Received for publication, June 3, 2014, and in revised form, August 8, 2014 Published, JBC Papers in Press, September 3, 2014, DOI 10.1074/jbc.M114.586834

Hemangi Patil[‡], Arjun Saha[‡1,2], Eugene Senda[‡1,3], Kyoung-in Cho[‡], MdEmdadul Haque[‡4], Minzhong Yu[§], Sunny Qiu[‡], Dosuk Yoon[‡], Ying Hao[‡], Neal S. Peachey[§¶‖], and Paulo A. Ferreira[‡5]**

*From the Departments of [‡]Ophthalmology and **Pathology, Duke University Medical Center, Durham, North Carolina 27710, the [§]Department of Ophthalmic Research, Cole Eye Institute, Cleveland Clinic Foundation, Cleveland, Ohio 44195, the [¶]Research Service, Cleveland Veterans Affairs Medical Center, Cleveland, Ohio 44106, and the [‖]Department of Ophthalmology, Cleveland Clinic Lerner College of Medicine of Case Western Reserve University, Cleveland, Ohio 44195*

Background: Ranbp2 and its Ran-GTP-binding domains' roles in RPE survival/function, a multidisease target, are elusive.
Results: RPE undergoes degeneration, disruptions of proteostasis of Ranbp2 partners, and blood-retinal barrier upon *Ranbp2* ablation. Impairment of selective Ran-GTP-binding domains of Ranbp2 suffices to promote RPE degeneration.
Conclusion: Ran GTPase regulation by Ranbp2 is vital to RPE.
Significance: Ranbp2-dependent targets/mechanisms with therapeutic potential in RPE degeneration are uncovered.

Retinal pigment epithelium (RPE) degeneration underpins diseases triggered by disparate genetic lesions, noxious insults, or both. The pleiotropic Ranbp2 controls the expression of intrinsic and extrinsic pathological stressors impinging on cellular viability. However, the physiological targets and mechanisms controlled by Ranbp2 in tissue homeostasis, such as RPE, are ill defined. We show that mice, *RPE-cre*::*Ranbp2*$^{-/-}$, with selective *Ranbp2* ablation in RPE develop pigmentary changes, syncytia, hypoplasia, age-dependent centrifugal and non-apoptotic degeneration of the RPE, and secondary leakage of choriocapillaris. These manifestations are accompanied by the development of F-actin clouds, metalloproteinase-11 activation, deregulation of expression or subcellular localization of critical RPE proteins, atrophic cell extrusions into the subretinal space, and compensatory proliferation of peripheral RPE. To gain mechanistic insights into what Ranbp2 activities are vital to the RPE, we performed genetic complementation analyses of transgenic lines of bacterial artificial chromosomes of *Ranbp2* harboring loss of function of selective Ranbp2 domains expressed in a *Ranbp2*$^{-/-}$ background. Among the transgenic lines produced, only *Tg*$^{RBD2/3*\text{-}HA}$::*RPE-cre*::*Ranbp2*$^{-/-}$-expressing mutations, which selectively impair binding of RBD2/3 (Ran-binding domains 2 and 3) of Ranbp2 to Ran-GTP, recapitulate RPE degeneration, as observed with *RPE-cre*::*Ranbp2*$^{-/-}$. By contrast, *Tg*$^{RBD2/3*\text{-}HA}$ expression rescues the degeneration of cone photoreceptors lacking Ranbp2. The RPE of *RPE-cre*::*Ranbp2*$^{-/-}$ and *Tg*$^{RBD2/3*\text{-}HA}$::*RPE-cre*::*Ranbp2*$^{-/-}$ share proteostatic deregulation of Ran GTPase, serotransferrin, and γ-tubulin and suppression of light-evoked electrophysiological responses. These studies unravel selective roles of Ranbp2 and its RBD2 and RBD3 in RPE survival and functions. We posit that the control of Ran GTPase by Ranbp2 emerges as a novel therapeutic target in diseases promoting RPE degeneration.

The retinal pigment epithelium (RPE)[6] is a critical component of the blood-retinal barrier and maintains retinal homeostasis by filtering damaging light, nourishing the neural retina, replenishing the 11-*cis*-retinal chromophore to photoreceptors, and phagocytizing damaged (photo-oxidized) outer segments of photoreceptors (1–3). RPE dysfunction underlies disparate diseases promoting RPE degeneration, such as atrophic and neovascular age-related macular degeneration (4–6),

* This work was supported, in whole or in part, by National Institutes of Health Grants EY019492, GM083165, and GM083165-04S1 (to P. A. F.), 2P30-EY005722 (to the Duke University Eye Center), and 5P30NS061789 (to the Duke Neurotransgenic Laboratory). This work was also supported by the Foundation Fighting Blindness and the Department of Veterans Affairs and an unrestricted award from Research to Prevent Blindness to Cleveland Clinic.

[S] This article contains supplemental Movies S1 and S2.

[1] Both authors contributed equally to this work.

[2] Present address: Duke Clinical Research Institute, Duke University Medical Center, Durham, NC 27710.

[3] Supported by a Duke University Dean's Summer Undergraduate Research Fellowship.

[4] Present address: Syngenta Biotechnology, Inc., Research Triangle Park, NC 27709.

[5] Supported in part by the Jules and Doris Stein Research to Prevent Blindness Professorship. To whom correspondence should be addressed: Duke University Medical Center, DUEC 3802, 2351 Erwin Rd., Durham, NC 27710. Tel.: 919-684-8457; Fax: 919-684-3826; E-mail: paulo.ferreira@duke.edu.

[6] The abbreviations used are: RPE, retinal pigment epithelium/epithelia; RBD, Ran-GTP-binding domain; BAC, bacterial artificial chromosome; EdU, 5-ethynyl-2′-deoxyuridine; miR, microRNA; ErbB1/2, epidermal growth factor receptor 1/2; ubc9, ubiquitin-conjugating enzyme 9; Mmp, matrix metalloproteinase; KBD, kinesin-binding domain; CLD, cyclophilin-like domain; 2D-DIGE, two-dimensional difference in-gel electrophoresis; ERG, electroretinogram; dc-ERG, direct current electroretinogram; qRT-PCR, quantitative real-time polymerase chain reaction; S1, S1(Rpn2) subunit of the 26 S proteasome; CY, cyclophilin domain; IF, immunofluorescence; IB, immunoblot(s); TRITC, tetramethylrhodamine isothiocyanate; AFC, *N*-acetyl-*S*-farnesyl-L-cysteine; cd, candela; FO, fast oscillation; SUMO, small ubiquitin-like modifier; Tg, transgenic; P*n*, postnatal day *n*; E*n*, embryonic day *n*.

bestrophinopathies (7), and various forms of retinal dystrophies (*e.g.* retinitis pigmentosa, Leber congenital amaurosis) (8–12). The cause-effect mechanisms of RPE degeneration are not understood, but they appear to arise from the interplay of multifactorial events impinging on heterogeneous genetic predispositions, noxious insults, and senescence that culminate with cytotoxicity to the RPE (13–21).

Emerging studies indicate that the modular and pleiotropic Ranbp2 (Ran (Ras-related nuclear protein)-binding protein 2) plays critical and cell type-dependent roles in cell survival, proliferation, or functions upon intrinsic or extrinsic pathological stressors. For example, haploinsufficiency of *Ranbp2* in an inbred genetic background confers neuroprotection to photoreceptor degeneration upon photo-oxidative stress and modulates glucose tolerance (22–24), whereas it increases the susceptibility of mice to 1-methyl-4-phenyl-1,2,3,6-tetrahydropyridine-elicited Parkinsonism (25) or carcinogenesis (26). Interestingly, RANBP2 is also a substrate for degradation by PARKIN (27, 28), whose impairment causes familial and sporadic Parkinson (29–31) or multisite oncogenesis (32, 33). Further, Ranbp2 loss in cones photoreceptors also elicits non-autonomous death of healthy rod photoreceptors (34), whereas asymptomatic mutations in human *RANBP2* predispose the basal ganglia to acute necrotic damage (*e.g.* encephalopathy) upon exposure to various infectious agents (35–37). A parsimonious model of the multifold activities of multimodular Ranbp2 arises from structure-function analyses of Ranbp2, whereby the dynamic recruitment and regulation of a functionally diverse set of cell-type selective and disease-prone substrates by distinct domains of Ranbp2 confer pleiotropic and distinct pathobiological roles to Ranbp2. However, it is unclear what substrates, activities, and modules of Ranbp2 control cell survival and responses to selective pathological stimuli.

Ranbp2 contains a tandem repeat of four Ran-GTP-binding domains ($RBD_{n=1-4}$), which are interspersed among other unrelated structural domains (38–40). The RBDs of Ranbp2 are highly homologous to the small Ranbp1 (Ran-binding protein 1), a Ran-GTP-binding protein highly conserved between yeast and humans (38–43), but Ranbp2 is not evolutionarily conserved (44). Contrary to evolutionary and system biology predictions (45, 46), loss of *Ranbp1* does not affect mouse viability (47), whereas *Ranbp2* ablation causes embryonic lethality (24, 26).

Ranbp2 comprises the cytoplasmic filaments emanating from nuclear pores in interphase cells (48). Ranbp2 has high affinity binding toward Ran-GTP and controls the nucleotide-bound state of Ran and association of nuclear shuttling substrates to Ran (43, 49, 50). Ran is a small and evolutionarily conserved Ras-related GTPase, which controls nucleocytoplasmic trafficking in interphase cells and spindle checkpoint signaling in proliferating cells (51–57). However, there are apparently conflicting reports, employing cell cultures, on whether regulation of nucleocytoplasmic trafficking and mitosis by Ranbp2 is essential for cellular function and/or survival. For example, down-modulation of Ranbp2 in cultured proliferating cells promotes mitotic abnormalities (58, 59), and mouse embryonic fibroblasts derived from hypomorph *Ranbp2* mice develop aneuploidy (26). By contrast, ectopic expression of Ranbp2 only with its N-terminal leucine-rich and first Ran-GTP-binding domains (RBD1) in mouse embryonic fibroblasts lacking endogenous *Ranbp2* suffices to rescue mitotic failure, cell death, and nuclear-cytoplasmic transport, even though such a Ranbp2 construct lacks an E3-ligase domain previously implicated in the control of mitotic progression (26, 60). Another study, however, suggests the need for other Ranbp2 domains in the nuclear shuttling of selective factors and in a manner that is independent of the regulation of Ran GAP and SUMO-E3 ligase activities by Ranbp2 (61). These studies contrast also with another employing immunoblocked Ranbp2 and Ranbp2-immunodepleted nuclei of *Xenopus* eggs that showed that Ranbp2 was dispensable for bulk nuclear transport (62). Collectively, these studies strengthen the notion that Ranbp2 and some of its domains control the nuclear shuttling of cell type-selective substrates, which determine cell survival and/or functions in a cell type-dependent manner.

To identify targets and mechanisms controlling RPE viability that may be amenable to pharmacological manipulations and therapeutic interventions in disease and aging-related conditions promoting RPE degeneration, we assessed the physiological roles of Ranbp2, its domains, and allied activities in RPE functions and survival. We carried out the conditional ablation of *Ranbp2* in the RPE and performed complementation genetic studies with transgenic BAC constructs of *Ranbp2* harboring selective impairments of its domains. We uncovered that *Ranbp2* is dispensable for RPE proliferation and that *Ranbp2* ablation promotes the progressive, autonomous, and non-autonomous degeneration of mature RPE cells and secondary impairment of choriocapillaris with manifestations reminiscent of those observed in neovascular age-related macular degeneration. Further, these pathological features and other molecular disturbances are retained selectively by the RPE upon mutations impairing specifically the binding of RBD2 and RBD3 of Ranbp2 to Ran-GTP but not loss of function of other domains of Ranbp2.

EXPERIMENTAL PROCEDURES

Generation of Mice with Constitutive Ablation of Ranbp2—Heterozygous $Ranbp2^{+/Gt(pGT0pfs)630Wcs}$ ($Ranbp2^{+/-}$) mice with constitutive disruption of the *Ranbp2* allele between exons 1 and 2 were described elsewhere (24). Homozygous $Ranbp2^{-/-}$ mice are embryonic lethal (24).

Generation of Mice with Selective Ablation of Ranbp2 in the RPE—Floxed *Ranbp2* ($Ranbp2^{flox/flox}$) (26, 34) or $Ranbp2^{+/Gt(pGT0pfs)630Wcs}$ ($Ranbp2^{+/-}$) were crossed to *PVMD2-rtTA*::*tetO-PhCMVcre* (*RPE-cre*) mice (63) to generate *RPE-cre*::$Ranbp2^{+/flox}$ or *RPE-cre*::$Ranbp2^{+/-}$ mice, respectively. *RPE-cre*::$Ranbp2^{+/flox}$ were crossed to $Ranbp2^{+/flox}$ or $Ranbp2^{+/-}$ to produce *RPE-cre*::$Ranbp2^{flox/flox}$ or *RPE-cre*::$Ranbp2^{-/flox}$ mice. No differences in RPE degeneration were observed between *RPE-cre*::$Ranbp2^{-/flox}$ and *RPE-cre*::$Ranbp2^{flox/flox}$; these mice are herein designated as *RPE-cre*::$Ranbp2^{-/-}$. In addition, we found that there were no differences in induction of *cre* and RPE degeneration between these lines in the absence and presence of doxycycline and mice fed with and without autoclaved chow (data not shown), an observation consistent with

the reported leakiness of the induction of *cre* in the RPE by the *tet-on* system (63).

Generation of Mice with Selective Ablation of Ranbp2 in Cone Photoreceptors—Mice with selective ablation of *Ranbp2* in M- and S-cone photoreceptors (*cone-cre*::*Ranbp2*$^{-/-}$) were generated by crossing floxed *Ranbp2* mice to *HRGP-cre* mice (*cone-cre*) as described elsewhere (34).

BAC Recombineering—A bacterial artificial chromosome (BAC) clone, RP24–347K24, from the mouse BAC library 24 of the BACPAC RPCI (Resource Center at the Children's Hospital Oakland Research Institute) was used to generate recombinant BAC constructs of *Ranbp2*. The BAC *Ranbp2* clone contains the complete *Ranbp2* gene with its upstream and downstream regulatory sequences (64). BAC constructs were generated by BAC recombineering upon sequential electroporation of *Escherichia coli* SW102 cells (gift from Neal G. Copeland) with BAC *Ranbp2* and ~500-bp amplicons containing point mutations in various domains of Ranbp2 exactly as described elsewhere (64). Recombinant BAC constructs were confirmed by dideoxy sequencing and NotI restriction mapping, purified with Nucleobond-BAC 100 kit (Macherey-Nagel, Germany) as per the manufacturer's instructions and diluted in microinjection buffer (10 mM Tris-HCl, pH 7.5, 0.1 mM EDTA, 30 μM spermine, 70 μM spermidine, 100 mM NaCl).

Generation of Transgenic Mice Expressing Recombinant BAC Ranbp2 Constructs in a Constitutive or Conditional Null Ranbp2 Background—To generate transgenic mice, recombinant BACs were injected into pronuclei followed by implantation into pseudopregnant females at the Duke Neurotransgenic Laboratory and Transgenic Mouse Facility of Duke University. F_0 founders, expressors, and transmission of BAC transgenes were identified by genomic PCR, RT-PCR, and immunoblot analyses. At least two independent lines were generated for each BAC transgenic construct. Positive F_0 transgenic founders of BAC *Ranbp2* constructs were mated with *Ranbp2*$^{Gt(pGT0pfs)630Wcs/-}$ (*Ranbp2*$^{+/-}$) (24) to generate BAC *Ranbp2* transgenic mice in a constitutive *Ranbp2*$^{-/-}$ background or with floxed *Ranbp2* (34) and *RPE-cre* mice (63) to generate BAC *Ranbp2* transgenic mice with selective ablation of endogenous *Ranbp2* in the RPE. BAC transgenic *Ranbp2* mice with the selective ablation of endogenous *Ranbp2* in M- and S-cone photoreceptors were generated by crossing transgenic mice to *cone-cre*::*Ranbp2*$^{-/-}$ (34). All BAC transgenic mice examined were hemizygous for the transgene allele and they were in a mixed genetic background. Mice were raised in a pathogen-free transgenic barrier facility at <70 lux and given *ad libitum* access to water and chow diet 5LJ5 (Purina, Saint Louis, MO).

Animal Study Protocols—Animal protocols were approved by the Institutional Animal Care and Use Committees of Duke University (A003-14-01) and Cleveland Clinic (2011-0580), and all procedures adhered to the National Academy of Sciences and ARVO guidelines for the Use of Animals in Vision Research.

Bright Field and Fluorescein Fundoscopy—Eyes of live mice were dilated by applying a drop of atropine sulfate ophthalmic solution (1%; Alcon Laboratories, Inc., Fort Worth, TX), followed by a drop of phenylephrine hydrochloride (10%; HUB Pharmaceuticals, LLC, Rancho Cucamonga, CA) after 5 min of atropine application. Bright field fundus pictures were taken with a Micron III imaging system (Phoenix Research Laboratories, Pleasanton, CA). Chorioretinal fluorescent angiography was carried out by intravenously injecting mice with FITC-dextran (0.5 g/kg body weight; Sigma, catalog no: FD10S) in phosphate-buffered saline in the tail vein. Fundus pictures of dilated eyes were taken immediately with a Micron III imaging system equipped with fluorescent filters. Fundus pictures were captured in recording mode for 30–60 s at ~22 frames/s and across different depths of the chorioretina; the best focused frames were selected for extraction.

Total RNA Isolation and qRT-PCR—Total RNA from the RPE was purified by TRIzol reagent (Invitrogen) or the Qiagen RNeasy minikit and treated with DNase (DNase I, 1 unit/μg total RNA) (Qiagen). Then mRNA was reverse transcribed using the SuperScript III first-strand synthesis system (Invitrogen). Quantitations of mRNA levels with gene-specific primers were carried out with cDNA equivalent to 2 ng of total RNA, SYBR Green PCR Master Mix, and the Eco real-time PCR system (Illumina Inc.). The data were analyzed using Eco real-time PCR system software version 5.0 (Illumina). The relative amount of transcripts was calculated by the $\Delta\Delta CT$ method and normalized to *Gapdh* ($n = 3–4$). Data were analyzed by Student's t test, and a p value of ≤ 0.05 was considered significant.

Antibodies—The primary antibodies used for immunofluorescence (IF) or immunoblots (IB) were the following: rabbit anti-Ranbp2 (W1W2/IR1 + 2-Ab#9; 1:50 (IF)) (64), mouse Ran GTPase (1:100 (IF), 1:4,000 (IB), BD Biosciences); mouse mAb414 against nuclear pore complex proteins Nup62, Nup153, and Nup358 (400 ng/ml (IB), 1:100 (IF), Covance, Emeryville, CA); mouse anti-HA (1:100 (IF), Abcam, Cambridge, MA); rabbit anti-L/M opsin number 21069 (1:500 (IF)) (34, 64); rabbit anti-S opsin (1:2,500 (IB), 1:100 (IF), Millipore, Temecula, CA); mouse anti-RANGAP1 (1:1,000 (IB), Invitrogen); rabbit anti-GAPDH antibody (1:500 (IB), Santa Cruz Biotechnology, Inc.); rabbit monoclonal anti-STAT3 (1:1,000 (IB), 1:50 (IF), Cell Signaling, Boston, MA); rabbit anti-pSTAT3 (1:50 (IF), Cell Signaling); mouse anti- Ubc9 (1:100 (IF), BD Biosciences); mouse anti-importin-β (1:200 (IF)), rabbit anti-exportin-1 (1:50 (IF), Santa Cruz Biotechnology); mouse anti-ErbB2 (1:50 (IF) Calbiochem); mouse anti-Rpe65 (retinal pigment epithelium-specific 65-kDa protein) (1:500 (IB), Santa Cruz Biotechnology); rabbit anti-19 S proteasome S1 (1:1000 (IB), Thermo Scientific, Rockford, IL); mouse anti-endophilin B1 (1–2 μg/ml (IB), Imgenex, San Diego, CA); rabbit anti-Arl2 (1:500 (IB), Proteintech); rabbit anti-serotransferrin (1:500 (IB) Proteintech); mouse anti-γ-tubulin (1:1,000 (IB), Abcam); mouse anti-Parp1 (1:2,000 (IB) BD Biosciences).

5-Ethynyl-2′-deoxyuridine (EdU) Labeling—For detection of proliferating RPE cells, mice received a daily bolus of EdU by intraperitoneal injection (100 μl of 1 mg ml^{-1} EdU) for 5 days with the exception of mice of P5 of age that received a daily dose of 50 μg/g body weight. Mice were sacrificed 7 days after the first injection. RPE flat mounts were fixed with 4% paraformaldehyde in 1× PBS solution for 15 min and washed once with 3% BSA in 100 mM PBS, followed by permeabilization with 100 mM PBS, pH 7.4, 0.5% Triton X-100 for 20 min. Then specimens

were incubated with the EdU detection mixture for 30 min as per the manufacturer's instructions (Click-iT® EdU Alexa 488 Imaging Kit, Invitrogen) and counterstained with DAPI as described elsewhere (25).

TUNEL Assay—TUNEL assays were performed on *en face* RPE with the DeadEnd Fluorometric TUNEL System (Promega, Madison, WI) as per the manufacturer's instructions and as described elsewhere (23, 64).

Immunohistochemistry—Collection and dissection of eyeballs and preparation of retinal flat mounts for immunohistochemistry with S-opsin and M-opsin antibodies were carried out as described previously (34, 64). For confocal imaging of *en face* RPE, eye globes were enucleated, and the anterior segment and the retina were removed carefully. The remaining RPE-choroid-sclera complex (eyecup) was flat-mounted with 4–6 radial cuts and fixed with 2% paraformaldehyde, 1× PBS overnight, washed with 1× PBS, permeabilized, and blocked in 0.2% Triton X-100, 5% normal goat serum for 24 h, followed by incubation with the primary antibodies for 36–48 h and washing in 1× PBS. Anti-goat, anti-rabbit, or anti-mouse AlexaFluor-488-, AlexaFluor-594-, or Cy5-conjugated secondary antibodies were incubated for 2 h. TRITC-conjugated phalloidin (1:1000; Sigma) was used to stain RPE cell junctions and F-actin intracellular condensation. Nuclei were counterstained with DAPI. Specimens were mounted and examined on glass slides with Fluoromount-G (Southern Biotech), and images were acquired with a Nikon $C1^+$ laser-scanning confocal microscope coupled with a LU4A4 launching base of four solid state diode lasers (407 nm/100 milliwatts, 488 nm/50 milliwatts, 561 nm/50 milliwatts, and 640 nm/40 milliwatts) and controlled by the Nikon EZC1.3.10 software (version 6.4).

Morphometric Analyses—Morphometric analyses of immunostained M- and S-cone photoreceptors were performed from three 127 × 127-μm image fields from each retinal region, and optical slices were three-dimensionally reconstructed for the whole length of outer segments (~25 μm, step size of 0.5 μm) from retinal flat mounts with the postacquisition Nikon Elements AR software (version 4.0). Photoreceptors and outer segments were tallied from the various retinal regions. Two-tailed equal or unequal variance *t* test statistical analysis was performed. $p \leq 0.05$ was defined as significant. Morphometric analyses of *en face* RPE cells were carried out also with Nikon Elements AR software (version 4.0) by tallying the number of cells and tracing the cell and nuclear boundaries for computation of areas in defined regions of the RPE. Central and peripheral RPE regions were arbitrarily defined as circular areas within a 1,500-μm radius of the optic nerve head and 1,000 μm from the ora serrata, respectively. Three-dimensional images of collapsed confocal stacks from *en face* RPE of *RPE-cre*::*Ranbp2*$^{+/+}$ (+/+) and *RPE-cre*::*Ranbp2*$^{-/-}$ (−/−) mice were generated by reconstructing optical slices that covered the whole depth of selected areas of *en face* RPE cells (112 × 112 × 8.4 μm (*x*, *y*, *z*) for +/+ and 112 × 112 × 19.25 μm for −/− and with a *z*-step size of 0.2 μm) from flat mounts of eyecups using Nikon Elements AR software.

Semithin Sections and Transmission Electron Microscopy—Semithin sections of posterior eyecups for light and transmission electron microscopy of ≥3 mice of each genotype were carried out as described elsewhere (34, 64). Briefly, eyeballs were fixed with 2% glutaraldehyde-paraformaldehyde, 0.1% cacodylate buffer, pH 7.2, and 0.5-μm sections along the vertical meridian were mounted on glass slides and stained with 1% methylene blue, and images were captured with an Axioplan-2 light microscope controlled by Axiovision release 4.6 and coupled to an AxioCam HRc digital camera (Carl Zeiss). Specimens for electron microscopy were postfixed in 2% osmium tetraoxide in 0.1% cacodylate buffer and embedded in Spurr resin. 60-nm-thick sagittal and tangential sections from the central regions of the RPE were cut with Leica Ultracut S (Leica Microsystems, Waltzer, Germany); stained with 2% uranyl acetate, 4% lead citrate; and imaged with a JEM-1400 transmission electron microscope (JEOL, Tokyo, Japan) coupled with an ORIUS 1000CCD camera.

Immunoblotting—RPE homogenates were prepared as described previously and with complete proteinase inhibitors (Roche Applied Science) and 10 mM iodoacetamide (Sigma). Protein concentration was measured by the BCA method using BSA as a standard (Pierce). Samples were resolved in standard 11 or 6% Hoefer (Holliston, MA) or premade 5–15% gradient Criterion SDS-polyacrylamide gels (Bio-Rad). Western blotting and antibody incubations were carried out as described previously (64). Whenever possible, blots were reprobed independently with multiple antibodies for analysis of proteostatic differences between genotypes. For densitometric analysis, integrated density values for the representative bands were normalized to the background and integrated density value of Gapdh. The band intensities were quantified with Metamorph version 7.0 (Molecular Devices). Data were analyzed by the two-tail *t* test with the assumption of unequal variance, and a *p* value of ≤0.05 was considered significant.

Caspase and Matrix Metalloproteinase (Mmp) Activity Assays—Caspase and Mmp activities were assayed essentially as described elsewhere (34). Briefly, RPE tissue was dissected from posterior mouse eyecups upon removal of the retina. RPE was homogenized with a Bullet Blender BBX24 homogenizer (Next Advance Inc.) and 0.5-mm zirconium oxide beads (Next Advance Inc.) at 4 °C. RPE was homogenized in radioimmune precipitation assay buffer to measure caspase activities (AnaSpec). For Mmp assays, radioimmune precipitation assay homogenates were diluted in Mmp assay buffers (AnaSpec). Retinal homogenates were centrifuged at 10,000 × *g* for 15 min at 4 °C. Supernatants were collected, and protein concentrations were determined by the BCA method using BSA as a standard. Caspase-profiling assays were performed with the following substrates: Ac-YVAD-AFC (SB1) and Ac-WEHD-FAC (SB2) for caspase-1, Ac-VDVAD-FAC (SB3) for caspase-2, Ac-IETD-FAC (SB4) for caspase-8, Ac-DEVD-FAC (SB5) and Z-DEVD-AFC (SB6) for caspase-3/7, Ac-LEHD-FAC (SB7) for caspase-9, and Ac-VEID-AFC (SB8) for caspase-6. Caspase assays were carried out with the Sensolyte AFC Caspase sampler kit as described elsewhere and according to the manufacturer's protocol (AnaSpec, Fremont, CA). Screening assays for Mmp activities of Mmp1, -2, -3, -7, -8, -9, -10, -11, -12, and -14 were carried out with the Sensolyte 520 generic Mmp assay kit as described elsewhere and according to the manufacturer's protocol (AnaSpec, Fremont, CA). Analytical assays with Mmp11 were carried out with 56 ng of RPE extract. Measurements of fluorescence were performed with SpectraMax M5 (Molecular

Devices, Sunnyvale, CA). Control measurements without RPE extracts under the same conditions were subtracted from the sample readings.

Two-dimensional Difference In-gel Electrophoresis (2D-DIGE) Protein Expression Profiling—RPE homogenates of *RPE-cre*::*Ranbp2*$^{+/+}$, *RPE-cre*::*Ranbp2*$^{-/-}$, and *Tg*$^{RBD2/3*\text{-}HA}$::*RPE-cre*::*Ranbp2*$^{-/-}$ mice of P14 of age were solubilized in radioimmune precipitation assay buffer followed by buffer exchange in two-dimensional lysis buffer (7 M urea, 2 M thiourea, 4% CHAPS, 30 mM Tris-HCl, pH 8.8) as described elsewhere (64). Homogenates were CyDye-labeled, and global protein profiling between nontransgenic and transgenic mice was carried out first by analytical and then preparative 2D-DIGE with Applied Biomics (Hayward, CA). Changes in protein expression levels with a 2-fold cut-off between genotypes were identified with DeCyder "in-gel" analysis software. Protein spots of interest were picked for protein identification by mass spectrometry (MALDI-TOF/TOF) and database search for protein ID. Data analyses and validation of mass spectrometry data were performed by the Ferreira laboratory.

GST Pull-downs with RPE Extracts—Nonidet P-40-solubilized extracts of RPE (60 μg) were prepared in the presence of 140 mM *N*-ethylmaleimide at 4 °C and incubated sequentially with 1.5 μM GST-RBD4 for 20 min at 24 °C and 50 μl of a 50% slurry of glutathione-S1-Sepharose 4B (GE Healthcare) equilibrated in incubation buffer (150 mM $NaCl_2$, 20 mM Tris, 1 mM EDTA, 0.4% Nonidet P-40, pH 8.0) for 1 h at 24 °C. Then Sepharose-4B-beads were precipitated at 800 $\times$ *g*, supernatants were saved, and Sepharose-beads were washed three times. Coprecipitates were eluted with Laemmli buffer containing 100 mM DTT and resolved by SDS-PAGE. Immunoblots were probed with anti-Ran GTPase antibody (1:1500; Covance).

Subcellular Fractionation of RPE—Subcellular fractionation of fresh RPE was performed by using the Qproteome Cell Compartment kit as per the manufacturer's instructions (Qiagen, Valencia, CA) with the exception that the cytosolic fraction was collected from total lysate of RPE after centrifugation at 100 $\times$ *g*. The cytosolic, membrane, and cytoskeletal fractions were pooled together and designated the non-nuclear fraction. Nuclear and non-nuclear fractions were solubilized in SDS sampler buffer and resolved by SDS-PAGE, and immunoblots were carried out with antibodies against Ran GTPase (BD Biosciences) and markers to nuclear and cytosolic fractions. The ratios of nuclear and non-nuclear fractions were calculated as integrated density values of the ratios of nuclear to total (nuclear and non-nuclear) fractions and non-nuclear to total (nuclear and non-nuclear) fractions, respectively. Average values of each fraction were compared between genotypes using a two-sample Student's *t* test with the assumption of unequal variance at the minimum significance level of 0.05.

Visual Electrophysiology—We studied mice using recording protocols designed to evaluate different aspects of outer retinal or RPE function. All studies were conducted following overnight dark adaptation, after which mice were anesthetized with ketamine (80 mg/kg) and xylazine (16 mg/kg) and placed on a temperature-regulated heating pad. Eye drops were used to dilate the pupil (2.5% phenylephrine HCl, 1% cyclopentolate, 1% tropicamide) and to anesthetize the corneal surface (1% proparacaine HCl).

Dark- and Light-adapted ERG—We used a conventional strobe-flash ERG protocol to evaluate responses of the outer retina (65). ERGs were recorded using a stainless steel wire active electrode referenced to a needle electrode placed in the cheek. A needle electrode placed in the tail served as ground lead. Responses were differentially amplified (0.3–1,500 Hz), averaged, and stored using a UTAS E-3000 signal averaging system (LKC Technologies, Gaithersburg, MD). White light strobe flashes were initially presented in darkness within a ganzfeld bowl. Stimuli were presented in increasing order, from a minimum of -3.6 log cd s/m^2 up to 2.1 log cd s/m^2. Cone ERGs were isolated by superimposing stimuli (-0.8 to 1.9 log cd s/m^2) upon a steady adapting field (20 cd/m^2). The amplitude of the *a*-wave was measured 7 ms after flash onset from the prestimulus baseline. The amplitude of the *b*-wave was measured from the *a*-wave trough to the peak of the *b*-wave or, if no *a*-wave was present, from the prestimulus baseline.

Direct Current Electroretinogram (dc-ERG)—We used a dc-ERG protocol to evaluate ERG components generated by the RPE (66). Responses were obtained from the left eye using a capillary tube with filament (BF100-50-10, Sutter Instrument Co., Novato, CA) that contacted the corneal surface and was filled with Hanks' buffered salt solution to make contact with an Ag/Ag Cl wire electrode. A similar electrode placed in contact with the right eye served as the reference. Responses were differentially amplified (direct current, 100 Hz), digitized at 20 Hz, and stored using LabScribe data recording software (iWorx, Dover, NH). White light stimuli were derived from an optical channel using a Leica microscope illuminator as the light source and delivered to the test eye with a 1-cm diameter fiber-optic bundle. The stimulus luminance was 2.4 log cd/m^2. Stimulus timing and duration were controlled at 7 min by a Uniblitz shutter system (Rochester, NY). The amplitude of the *c*-wave was measured from the prestimulus baseline to the peak of the *c*-wave. The amplitude of the fast oscillation (FO) was measured from the *c*-wave peak to the trough of the FO. The amplitude of the light peak was measured from the FO trough to the asymptotic value. The off-response amplitude was measured from the light peak value just prior to stimulus light offset to the peak of the initial component.

ERG Statistical Analysis—Two-way repeated measures analyses of variance were used to analyze luminance-response functions for measures of dark- and light-adapted ERG amplitude. Student's *t* tests were used to analyze the major components of the dc-ERG. $p \leq 0.05$ was defined as significant.

RESULTS

Conditional Ablation of Ranbp2 in the RPE—To assess the role(s) of Ranbp2 in the RPE, we generated mice, *RPE-cre*::*Ranbp2*$^{-/-}$, with selective ablation of *Ranbp2* in the RPE (Fig. 1*A*) (63). In accord with a prior report (63), we found that transcriptional induction of *cre* in the RPE of our lines began at E16 and was phased out by approximately P35 (Fig. 1*B*). Cre protein expression was not high enough to be detected by immunoassays at any age. The temporal and transcriptional expression of *cre* matched the cre-mediated excision of exon 2 (*Ranbp2*$^{\Delta E2}$)

as early as E16 (Fig. 1*B*). To assess further *cre* expression in the RPE during development and without potential confounding factors arising from RPE degeneration, we monitored quantitatively the developmental and transcriptional profile of *cre* in the RPE by qRT-PCR in a wild-type background. When compared with P14 mice, *cre* expression was 5-fold higher and strongly reduced by 0.75-fold at P4 and 24 weeks of age, respectively (Fig. 1*C*). Analyses of mRNA and protein levels of Ranbp2 in the RPE between *RPE-cre*::*Ranbp2*$^{+/+}$ and *RPE-cre*::*Ranbp2*$^{-/-}$ of P35 of age showed that their levels were decreased by ~75% in *RPE-cre*::*Ranbp2*$^{-/-}$ (Fig. 1*D*). By contrast, transcriptional levels of *Ranbp2* in isolated retinas remained unchanged between

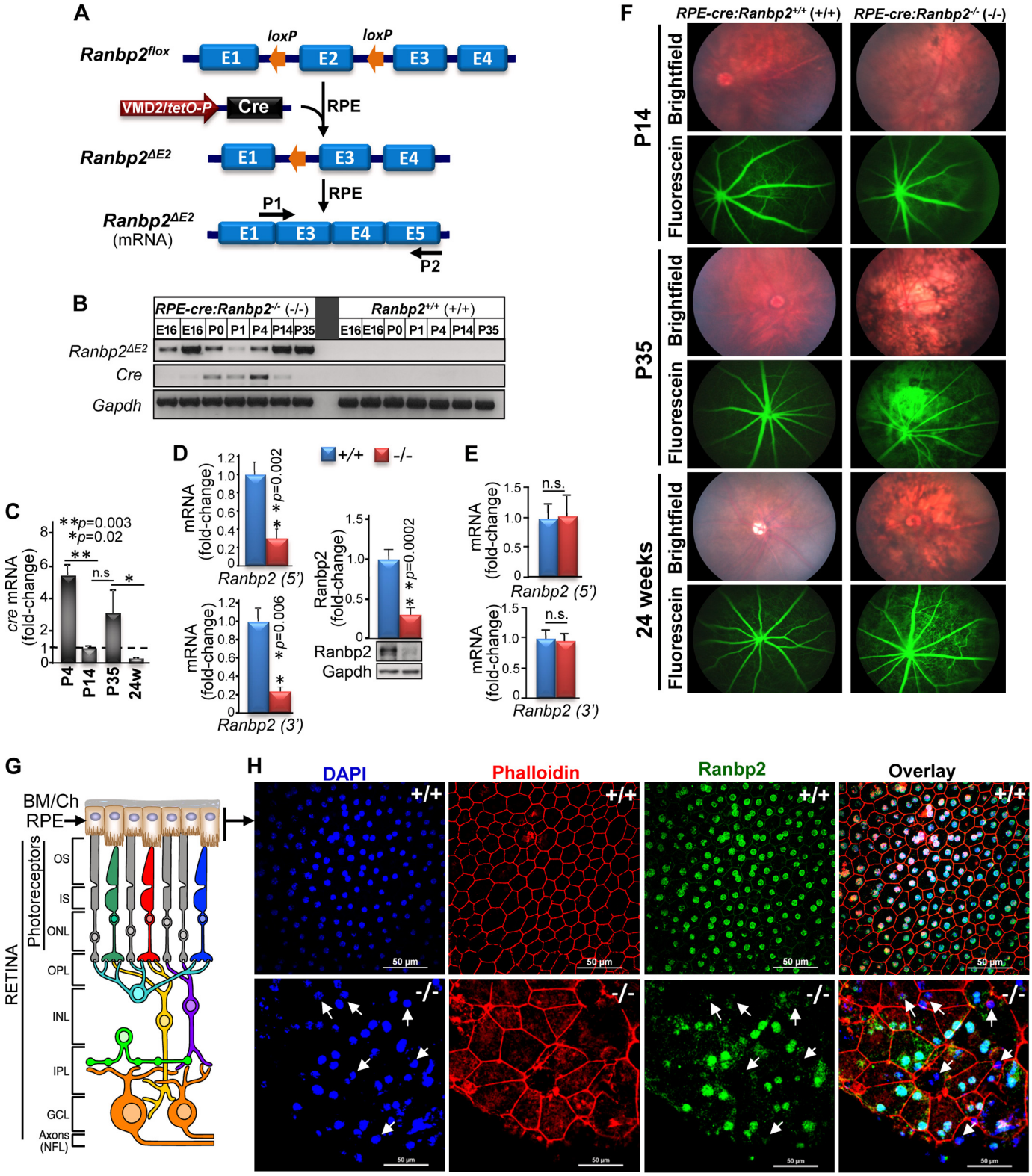

RPE-cre::*Ranbp2*$^{+/+}$ and *RPE-cre*::*Ranbp2*$^{-/-}$ (Fig. 1*E*), and transcriptional expression of *cre* was not detected in the retina in any genotype (data not shown). These data indicate that ablation of *Ranbp2* in *RPE-cre*::*Ranbp2*$^{-/-}$ mice is selective to the RPE.

Ablation of Ranbp2 Promotes RPE Degeneration and Choriocapillaris Leakage—We found that mice developed RPE degeneration, but about one-third of *RPE-cre*::*Ranbp2*$^{-/-}$ mice also developed Parkinsonian tremors at ~4 weeks of age (supplemental Movie S1), a manifestation that was reminiscent to that of the increased susceptibility of inbred *Ranbp2*$^{+/-}$ mice to 1-methyl-4-phenyl-1,2,3,6-tetrahydropyridine neurotoxicity (25). Hence, the Parkinsonian tremor, which co-segregated always with *RPE-cre*::*Ranbp2*$^{-/-}$, is a trait with incomplete penetrance (Yates' $\chi^2 = 14.89$, Yates' $p < 0.0001$). The Parkinsonian tremors of *RPE-cre*::*Ranbp2*$^{-/-}$ mice became increasingly severe, and these mice typically did not survive beyond 8 weeks of age (supplemental Movie S2). Mice with Parkinsonian tremors were excluded from analyses in this study, but such manifestation probably arises from the low or discrete but still poorly characterized expression in the brain of *VMD2* (67), whose promoter drives *cre*-mediated ablation of *Ranbp2* in this study.

To clinically characterize RPE degeneration, we carried out bright field and fluorescein fundus photography of live *RPE-cre*::*Ranbp2*$^{+/+}$ and *RPE-cre*::*Ranbp2*$^{-/-}$ mice at different ages (Fig. 1*F*). Bright field fundoscopy showed extensive degeneration of the RPE of *RPE-cre*::*Ranbp2*$^{-/-}$ as early as P14. This was followed by the prominent extravasation of FITC-labeled dextran from the choriocapillaris and their hyperfluorescence at ~P35 that persisted to at least 24 weeks of age (Fig. 1*F*). Changes in retinal vascular permeability appear unremarkable. Then we examined the overall *en face* morphological organization of the RPE and Ranbp2 expression in this tissue of P35 mice by confocal microscopy (Fig. 1, *G* and *H*). Wild-type *RPE-cre*::*Ranbp2*$^{+/+}$ mice (+/+) present phalloidin-labeled RPE cells with well tessellated and demarked hexagonal cell boundaries and Ranbp2-immunolabeled nuclei (Fig. 1*H*, *top panel*). By contrast, the RPE of *RPE-cre*::*Ranbp2*$^{-/-}$ (−/−) showed morphologically heterogeneous subpopulations of RPE cells with prominent hypoplasia, loss of hexagonal cellular architecture and junctional integrity, and DAPI$^+$ nuclei of RPE cells with and without or weak Ranbp2 immunostaining (Fig. 1*H*, *bottom panel*, *arrows*). This observation is concordant with the chimeric loss of Ranbp2 expression and chimeric cre-mediated recombination of the *RPE-cre* line reported by others (63, 68).

To assess in detail the onset and progression of RPE degeneration, we performed morphometric analyses of RPE of *RPE-cre*::*Ranbp2*$^{+/+}$ and *RPE-cre*::*Ranbp2*$^{-/-}$ mice from P1 to 24 weeks of age (Fig. 2). In comparison with *RPE-cre*::*Ranbp2*$^{+/+}$, changes in RPE cell densities of *RPE-cre*::*Ranbp2*$^{-/-}$ became noticeable in the central and peripheral regions of the RPE by P14 and P35, respectively, when there was a progressive decrease of cell density with aging (Fig. 2, *A* and *B*). Hypoplasia became noticeable in the central region of the RPE of *RPE-cre*::*Ranbp2*$^{-/-}$ at P4, and it became extremely severe in the central and peripheral RPE by P35 and 24 weeks of age, respectively (Fig. 2, *A* and *C*). There was also a progressive increase of the nuclear areas of RPE cells of *RPE-cre*::*Ranbp2*$^{-/-}$ as early as P4 and P35 in the central and peripheral RPE, respectively (Fig. 2*D*). Another hallmark and pathological feature of RPE cells of *RPE-cre*::*Ranbp2*$^{-/-}$ was polyploidization. Wild-type RPE cells were always either mono- or binucleated, whereas those of *RPE-cre*::*Ranbp2*$^{-/-}$ presented syncytia with up to four nuclei. Polyploidy became visible at P14 and remained restricted to the central RPE at older ages (Fig. 2*E*). The development of atrophic cells was also observed in *RPE-cre*::*Ranbp2*$^{-/-}$. These were typically surrounded by large cells in *RPE-cre*::*Ranbp2*$^{-/-}$. Most atrophic RPE cells presented F-actin condensation with prominent F-actin clouds (69), which were characterized by strong phalloidin-stained F-actin rings.

Ranbp2 is implicated in arresting mitotic progression (26, 58, 59), a process that is critical to support the repair capacity of the RPE, presumably due to differences in regenerative capacity between the central and peripheral RPE (70). Hence, we examined also changes of the proliferative capacity of the RPE at different ages between *RPE-cre*::*Ranbp2*$^{+/+}$ and *RPE-cre*::*Ranbp2*$^{-/-}$ mice. Quantitative analyses of whole RPE for the incorporation in nuclei of the thymidine analog, EdU, showed that *RPE-cre*::*Ranbp2*$^{-/-}$ had an increased number of proliferating cells across all ages tested. Interestingly, the RPE of both genotypes presented increased proliferation in the central region compared with its peripheral region at P5, when most RPE cells exit mitosis, but this proliferative increase became most prominent in the peripheral region of the RPE in *RPE-cre*::*Ranbp2*$^{-/-}$ at P15 and P42 (Fig. 2*F*).

FIGURE 1. **Genetic ablation of *Ranbp2* in the RPE promotes RPE degeneration and leakage of choriocapillaris.** *A*, diagram of *Ranbp2* gene structure before and after cre-mediated recombination. Cre is under the control of the *VMD2* promoter, which leads to the excision of exon 2 of *Ranbp2* selectively in the RPE. P1 and P2 are primers used for monitoring *Ranbp2* mRNA with a deletion of exon 2 (Δ*E2*). *B*, developmental and transcriptional expression profile in the RPE of *cre* and *Ranbp2* lacking exon 2. Excision of exon 2 was detectable as early as E16 and up to P35. *C*, temporal profile of *cre* mRNA expression measured by qRT-PCR from RPE of *RPE-cre*::*Ranbp2*$^{+/+}$ (+/+). Fold change in *cre* mRNA is shown relative to mice of P14 of age. In comparison with P14, there was a significant decrease of *cre* expression in the RPE between P4 and 24-week-old mice. In comparison with P14, P4 and 24-week-old mice present a 5- and 0.25-fold change of *cre* levels, respectively. *D* and *E*, mRNA and protein levels of Ranbp2 measured by qRT-PCR and quantitative immunoblot analysis, respectively, in RPE (*D*) and retina (*E*) of *RPE-cre*::*Ranbp2*$^{+/+}$ (+/+) and *RPE-cre*::*Ranbp2*$^{-/-}$ (−/−). *Ranbp2* mRNA was measured independently with two sets of primer pairs against the 5′- and 3′-ends of *Ranbp2*. In the RPE, −/− mice have an 80% reduction of mRNA and protein levels of Ranbp2 compared with +/+ mice (*D*). In the retina, *Ranbp2* mRNA levels are similar between genotypes (*E*). *F*, bright field fundoscopy and fluorescein (FITC)-labeled dextran angiograms of *RPE-cre*::*Ranbp2*$^{+/+}$ (+/+) and *RPE-cre*::*Ranbp2*$^{-/-}$ (−/−) at P14, P35, and 24 weeks of age. Bright field fundoscopy shows RPE degeneration at all ages, whereas angiograms show profuse extravasation of FITC-dextran from choriocapillaris beginning at P35. *G*, diagram of chorioretinal structure and organization of the choroid, RPE, and retinal neurons. *H*, *en face* confocal images of RPE of *RPE-cre*::*Ranbp2*$^{+/+}$ (+/+) and *RPE-cre*::*Ranbp2*$^{-/-}$ (−/−) immunostained for Ranbp2 and counterstained with DAPI and phalloidin. Compared with +/+, many DAPI$^+$ nuclei of RPE cells of −/− mice lack immunostaining of Ranbp2 (*arrows*), and RPE shows derangement of tessellated RPE cells, which become large and atrophic and abnormal in shape and present F-actin condensation. *BM/Ch*, Bruch's membrane/choroid; *OS*, outer segments of rod and cone photoreceptors; *IS*, inner segments of rod and cone photoreceptors; *ONL*, outer nuclear layer; *OPL*, outer plexiform layer; *INL*, inner nuclear layer; *IPL*, inner plexiform layer; *GCL*, ganglion cell layer. Data represent the mean ± S.D. (*error bars*), $n = 4$ (*C*, *D*, and *E*); *n.s.*, non-significant; +/+, *RPE-cre*::*Ranbp2*$^{+/+}$; −/−, *RPE-cre*::*Ranbp2*$^{-/-}$; *scale bar*, 50 μm (*H*).

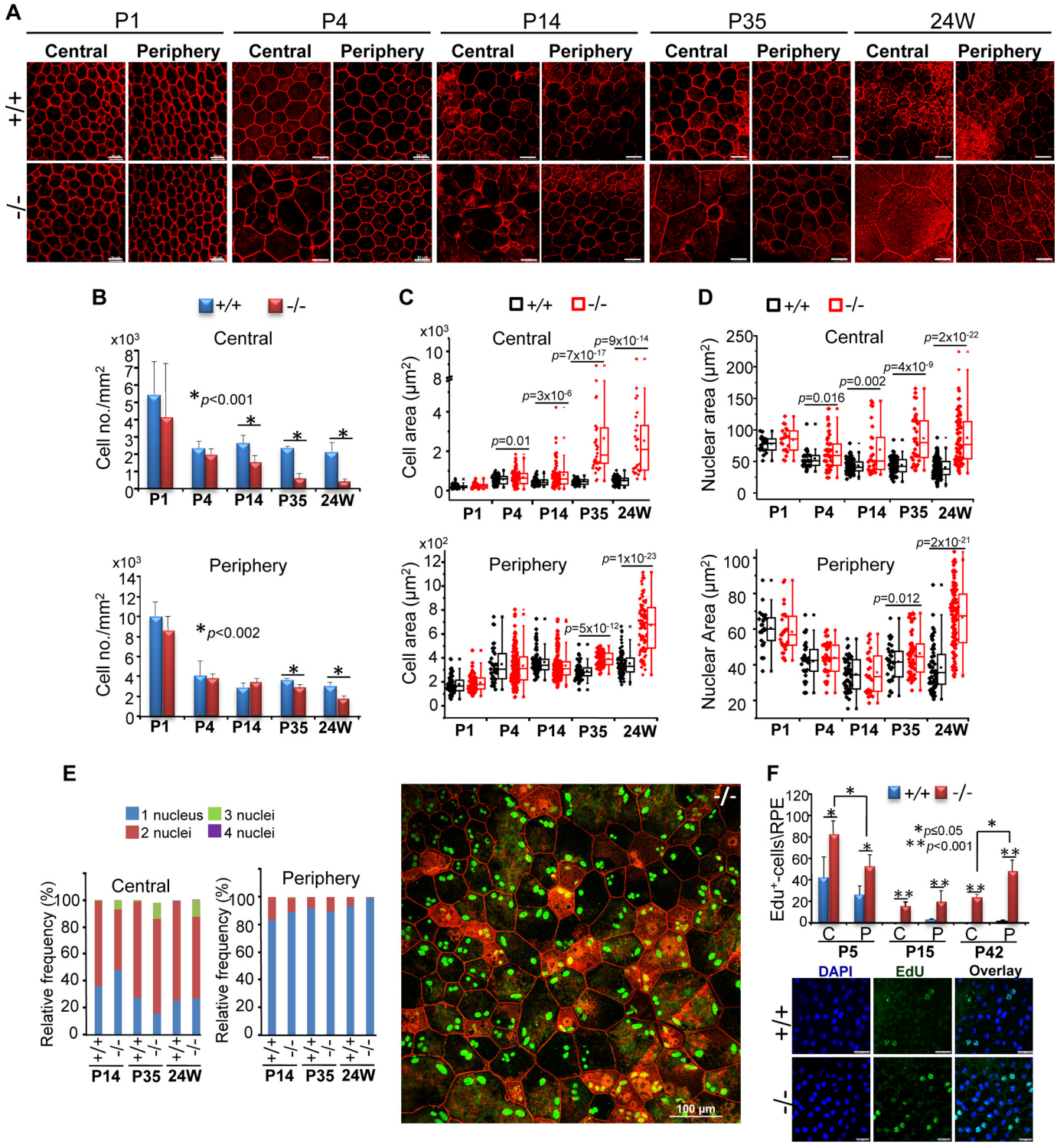

FIGURE 2. **Morphometric analyses of onset and progression of RPE degeneration and proliferation.** *A*, confocal images of *en face* central and peripheral RPE of *RPE-cre*::*Ranbp2*$^{+/+}$ (+/+) and *RPE-cre*::*Ranbp2*$^{-/-}$ (−/−) stained with phalloidin at different ages. Degeneration of the RPE becomes clearly noticeable in the central and peripheral RPE by P14 and P35, respectively. Shown are morphometric analyses of cell density (*B*), cell area (*C*), nuclear area (*D*), frequency of multinucleation (*E*) of central and peripheral RPE of *RPE-cre*::*Ranbp2*$^{+/+}$ (+/+) and *RPE-cre*::*Ranbp2*$^{-/-}$ (−/−) at different ages. The image *beside* the bar graphs in *E* shows *en face* central RPE of −/− immunostained for Ranbp2 (*green*) and counterstained with phalloidin (*red*). Multiple cells present three and four nuclei, and atrophic cells present with F-actin clumping and F-actin clouds (actin-rich and ringlike structures). *F*, morphometric analyses of EdU^{+}-nuclei of central (*C*) and peripheral (*P*) RPE of *RPE-cre*::*Ranbp2*$^{+/+}$ (+/+) and *RPE-cre*::*Ranbp2*$^{-/-}$ (−/−) at different ages. *Below* the graph is a representative image of EdU-labeled and DAPI-counterstained RPE of +/+ and −/− mice at P15. Compared with +/+, RPE of −/− mice present an increased number of EdU^{+}-RPE cells across all ages; EdU^{+} cells decrease between P5 and P15, and they increase at P42 predominantly in the peripheral RPE. Data represent the mean ± S.D. (*error bars*) (*B* and *F*); dot-box plot analyses are shown in *C* and *D*, and statistical analysis was done using a Mann-Whitney *U* test at a significance level of 0.05; $n = 4$ (P1), $n = 4$ (P4), $n = 5$ (P14), $n = 3$ (P35, 24 weeks) (*D* and *E*); +/+, *RPE-cre*::*Ranbp2*$^{+/+}$; −/−, *RPE-cre*::*Ranbp2*$^{-/-}$; *scale bar*, 20 µm (*A* and *F*).

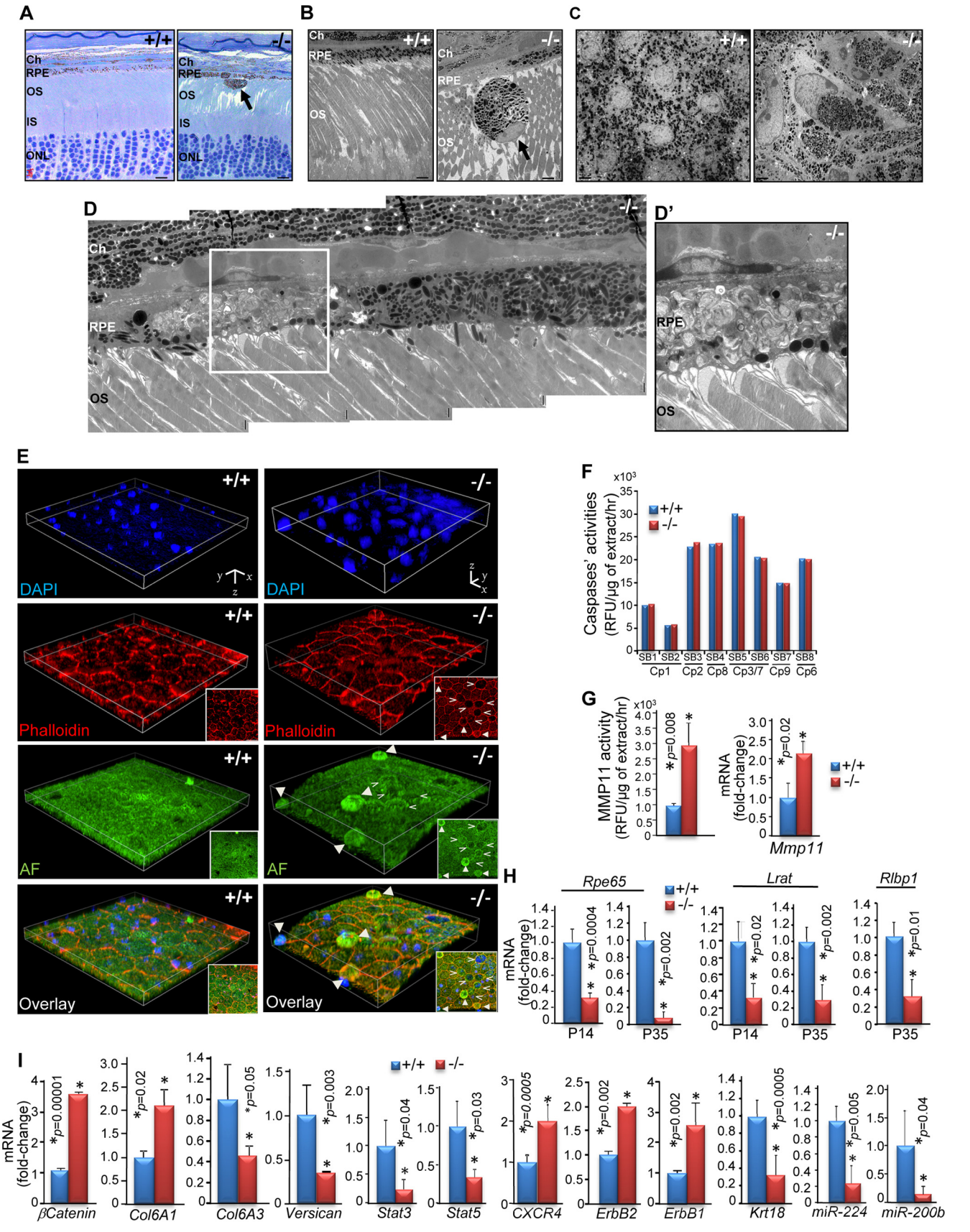
A
+/+
-/-
Ch
RPE
OS
IS
ONL
B
C
D
D'
E
DAPI
Phalloidin
AF
Overlay
F
Caspases' activities (RFU/µg of extract/hr)
x10³
+/+
-/-
SB1 SB2 SB3 SB4 SB5 SB6 SB7 SB8
Cp1 Cp2 Cp8 Cp3/7 Cp9 Cp6
G
MMP11 activity (RFU/µg of extract/hr)
mRNA (fold-change)
*p=0.008
*p=0.02
Mmp11
H
Rpe65
Lrat
Rlbp1
*p=0.0004
*p=0.002
*p=0.02
*p=0.002
*p=0.01
P14
P35
I
βCatenin
Col6A1
Col6A3
Versican
Stat3
Stat5
CXCR4
ErbB2
ErbB1
Krt18
miR-224
miR-200b
*p=0.00001
*p=0.02
*p=0.05
*p=0.003
*p=0.04
*p=0.03
*p=0.0005
*p=0.002
*p=0.002
*p=0.0005
*p=0.005
*p=0.04

Cellular and Molecular Mechanisms Underlying RPE Degeneration of RPE-cre::Ranbp2$^{-/-}$ Mice—To elucidate the cellular and molecular mechanisms of RPE degeneration of *RPE-cre*::*Ranbp2*$^{-/-}$ mice, we performed ultrastructural, confocal, biochemical, and gene expression analyses of RPE of *RPE-cre*::*Ranbp2*$^{+/+}$ and *RPE-cre*::*Ranbp2*$^{-/-}$ mice. In comparison with *RPE-cre*::*Ranbp2*$^{+/+}$, light and electron microscopy analyses of semithin radial sections of mouse eyecups revealed widespread RPE regions of hyperpigmentation and hypopigmentation and evasion of atrophic RPE cells into the subretinal space of *RPE-cre*::*Ranbp2*$^{-/-}$ mice (Fig. 3, *A–C*). These manifestations were also visible in flat mount and tangential sections of *RPE-cre*::*Ranbp2*$^{-/-}$ RPE cells, which presented strong intracellular clustering of melanosomes and nuclei with irregular shape (Fig. 3*C*). Patchy areas of accumulations of membranous debris of the outer segment of photoreceptors in the lumen of dysmorphic RPE cells were also visible in RPE cells of *RPE-cre*::*Ranbp2*$^{-/-}$, but photoreceptors had otherwise normal outer segments (Fig. 3, *D* and *D′*). Widespread apical extrusions of RPE cells to the subretinal space were also confirmed by three-dimensional confocal microscopy of *en face* RPE attached to the eyecup (Fig. 3*E*, *filled arrowheads*). Further, the extruded cells were atrophic and became rounded prior to and upon extrusion, as seen by two-dimensional optical sections (Fig. 3*E*, *inset pictures*, *filled* and *open arrowheads*). Further, RPE cell extrusion and/or degeneration promoted the recruitment of morphologically distinct CD45^{+} CD11b^{-} macrophage/glia cells (data not shown).

We showed previously that ablation of *Ranbp2* in cone photoreceptor neurons triggers the activation of metalloproteinase-11 (Mmp11) and caspase-7 without apoptosis (34). To gain insights into the mechanisms of cell death of RPE, we carried out TUNEL, caspase, and Mmp11 assays with RPE of *RPE-cre*::*Ranbp2*$^{+/+}$ and *RPE-cre*::*Ranbp2*$^{-/-}$ mice. We did not detect any TUNEL^{+} cells in any genotype. Then we screened RPE extracts for activities against substrates of various caspases and metalloproteinases. We did not find differences in activations of multiple caspases in the RPE between genotypes (Fig. 3*F*). In comparison with *RPE-cre*::*Ranbp2*$^{+/+}$ mice, however, the RPE extracts of *RPE-cre*::*Ranbp2*$^{-/-}$ exhibited a 3-fold increase in Mmp11 activity but not of any other metalloproteinase tested (Fig. 3*G*, *left graph*). This increase in Mmp11 activity was accompanied also by a 2-fold transcriptional increase of *Mmp11* (Fig. 3*G*, *right graph*).

The RPE plays a critical role in the visual cycle, because it contains the enzymatic machinery to regenerate *all-trans*-retinal to 11-*cis*-retinal after the release of *all-trans*-retinal from photoreceptors (2). The reisomerization of *all-trans*-retinal requires enzymes, such as Rpe65 (retinal pigment-specific 65-kDa protein) and Lrat (lecithin-retinol acyltransferase) (71). To assess the role of Ranbp2 in the modulation of the visual cycle, we measured the transcriptional levels of *Rpe65*, *Lrat* and *Rlbp1* (retinaldehyde-binding protein 1) in the RPE between *RPE-cre*::*Ranbp2*$^{+/+}$ and *RPE-cre*::*Ranbp2*$^{-/-}$ mice at P14 and P35. *RPE-cre*::*Ranbp2*$^{-/-}$ presented much lower levels of *Rpe65*, *Lrat*, and *Rlbp* than *RPE-cre*::*Ranbp2*$^{+/+}$ mice as early as P14 (Fig. 3*H*). We also examined the transcriptional levels of genes critical to RPE functions, such as those implicated in mediating cell junction to nuclear signaling (β-catenin) (72), extracellular matrix remodeling and/or adhesion (collagen VI α1/3, versican) (73, 74), inflammation and cytokine signaling (*Stat3*, *Stat5*, and *CXCR4* (C*X*C chemokine receptor type 4 (fusin/CD184)) (64, 75, 76), receptor tyrosine kinase signaling (*ErbB1/2*) (22, 77), and markers of RPE (cytokeratin 18, *miR-224*, and *miR-200b*) (78). We found that RPE of *RPE-cre*::*Ranbp2*$^{-/-}$ mice exhibit strong deregulation of the transcriptional expression of all these genes at P14 (Fig. 3*I*).

Ranbp2 modulates the nucleocytoplasmic shuttling of a set of partners that are functionally diverse, due to the direct association of distinct domains of Ranbp2 with nuclear import and export receptors, such as importin-β and exportin-1/Crm1, respectively, and other shuttling substrates (22, 48, 64, 79). Hence, we examined changes in the subcellular distribution of some Ranbp2 partners in the RPE between *RPE-cre*::*Ranbp2*$^{+/+}$ and *RPE-cre*::*Ranbp2*$^{-/-}$ mice (Fig. 4, *A–F*). The nuclear localization of importin-β was dependent on the nuclear localization of Ranbp2, because DAPI^{+}-Ranbp2^{-}-nuclei lacked importin-β staining (Fig. 4*A*). By contrast, expor-

FIGURE 3. **Subcellular and molecular changes of RPE degeneration in *RPE-cre*::*Ranbp2*$^{-/-}$.** *A*, radial semithin sections of P35 eyecups stained with methylene blue show regions of hyperpigmentation and hypopigmentation of RPE and escape of a hyperpigmented and atrophic RPE cell into the subretinal space of *RPE-cre*::*Ranbp2*$^{-/-}$ (−/−). There were no prominent morphological changes of the outer retina with the exception of the disruption of outer segment organization, where few escaping and atrophic RPE cells were found. *OS*, outer segments of rod and cone photoreceptors; *Ch*, choroid; *IS*, inner segments of rod and cone photoreceptors; *ONL*, outer nuclear layer. *B*, ultrastructural images of a radial section of choroid/RPE and outer segments of photoreceptors of P35 *RPE-cre*::*Ranbp2*$^{+/+}$ (+/+) and *RPE-cre*::*Ranbp2*$^{-/-}$ (−/−) showing regions of hyperpigmentation and hypopigmentation of RPE and escape of a hyperpigmented and atrophic RPE cell into the subretinal space of −/− mice. *C*, ultrastructural images of tangential sections of flat mounts of RPE attached to the posterior eye segment. The RPE cells are tessellated, melanosomes are uniformly dispersed, and nuclei are round in +/+ of P35, whereas nuclei and cells of RPE have abnormal shapes and the melanosomes are clumped in age-matched −/−. *D*, high power magnification ultrastructure of a radial section of choroid/RPE and outer segments of photoreceptors in −/− of P35 showing a region of hyperpigmentation and another of hypopigmentation with accumulation of outer segments membrane debris in dysfunctional RPE cells. Outer segments of photoreceptors look normal. *D′*, a higher magnification of the *inset* in *D*. *E*, three-dimensional images of collapsed confocal stacks from *en face* RPE of +/+ and −/− mice at P35 showing the even surface and tessellated organization of RPE cells in +/+, whereas various stages of RPE cell extrusions (*filled arrowheads*) can be discerned in −/− mice. *Insets*, two-dimensional images of three-dimensional images, showing the presence of multiple round-shaped cells in −/−. A *pit* is seen at the *center* of the three-dimensional image, where the round-shaped RPE cells became confluent (*open arrowheads*). Autofluorescence (*AF*) contributed by nonspecific staining at 488 nm was used for surface mapping of RPE. *F*, caspases' activities against caspase-specific substrates (SB1–8) in RPE homogenates. There were no differences of activities of multiple caspases in the RPE between +/+ and −/− mice at P35. *G*, Mmp11 activity of RPE extracts and transcriptional levels of *Mmp11* of +/+ and −/− mice. There is 3-fold higher Mmp11 activity and a 2.2-fold transcriptional increase of *Mmp11* levels in RPE of −/− at P35 in comparison with age-matched +/+. *H*, compared with +/+, the RPE of −/− mice exhibit a strong decrease of mRNAs encoding visual cycle proteins, such as Rpe65, Lrat, and Rlbp, at P14 and P35. *I*, transcriptional deregulation of β-catenin, collagen type 6A1 and A3, versican, *Stat3*, *Stat5*, *CXCR4*, *ErbB2/1*, *Krt18* (keratin 18), *miR-244*, and *miR-200b* in RPE of −/− compared with +/+ mice. Data represent the mean ± S.D. (*error bars*), $n = 4$ (*F–I*); +/+, *RPE-cre*::*Ranbp2*$^{+/+}$; −/−, *RPE-cre*::*Ranbp2*$^{-/-}$. *AF*, autofluorescence. *Scale bars*, 10 μm (*A*), 4 μm (*B*), 2 μm (*C*), 1 μm (*D*). Stack cuboidal measures for +/+ were as follows: $x, y = 112$ μm; $z = 8.4$ μm (*E*). Stack cuboidal measures for −/− were as follows: $x, y = 112$ μm; $z = 19.25$ μm (*E*).

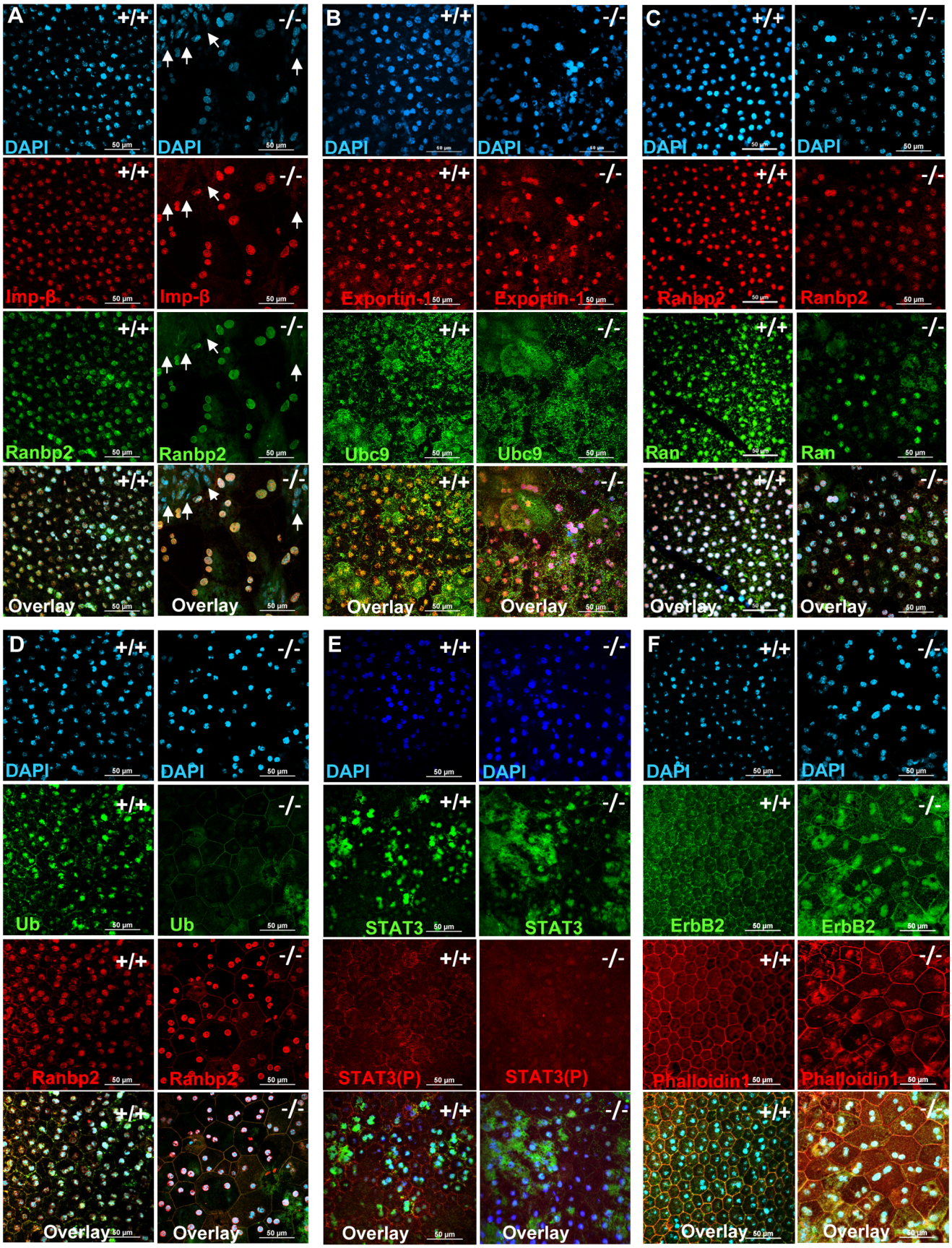
A
+/+
-/-
DAPI
Imp-β
Ranbp2
Overlay
B
Exportin-1
Ubc9
C
Ranbp2
Ran
D
Ub
E
STAT3
STAT3(P)
F
ErbB2
Phalloidin1
50 μm

tin-1/Crm1 was present in all DAPI$^+$ nuclei of both genotypes, whereas Ubc9 distribution was strongly affected across RPE cells of *RPE-cre*::*Ranbp2*$^{-/-}$ (Fig. 4*B*). In particular, Ubc9 was predominantly localized in the nucleus and membrane junctions of *RPE-cre*::*Ranbp2*$^{+/+}$, whereas ablation of *Ranbp2* promoted small foci of pan-cytosolic aggregates of Ubc9 (Fig. 4*B*). Ran GTPase was uniformly localized in the nucleus of *RPE-cre*::*Ranbp2*$^{+/+}$, whereas in *RPE-cre*::*Ranbp2*$^{-/-}$, such localization was not uniform across Ranbp2$^+$ nuclei. Ranbp2 was also shown to modulate various facets of the ubiquitin-proteasome system and ubiquitin homeostasis in the absence or presence of stressors (22, 64, 80). Compared with *RPE-cre*::*Ranbp2*$^{+/+}$, *RPE-cre*::*Ranbp2*$^{-/-}$ presented a strong redistribution of ubiquitin from the nuclear to the cytosolic compartment (Fig. 4*D*). The localizations of the Ranbp2 partners, Stat3 and activated/phosphorylated Stat3, Stat3(P) (64), were also assessed. Stat3 was localized to the nucleus in both genotypes, but ablation of *Ranbp2* caused a strong decrease of Stat3(P) at the membrane junctions compared with *RPE-cre*::*Ranbp2*$^{+/+}$ (Fig. 4*E*). Finally, ErbB2, another partner of Ranbp2 (22, 81), was present in the nucleus and strongly in the plasma membrane of *RPE-cre*::*Ranbp2*$^{+/+}$, but *RPE-cre*::*Ranbp2*$^{-/-}$ presented loss of ErbB2 at the membrane junctions and sequestration of ErbB2 in cytosolic F-actin clouds (Fig. 4*F*).

Generation of Transgenic Ranbp2 Mouse Lines Expressing Mutations in Selective Domains of Ranbp2 in a Constitutive Ranbp2$^{-/-}$ *Background*—The findings show that loss of function of pleiotropic Ranbp2 promotes profound molecular and subcellular imbalances of Ranbp2 partners and homeostasis of the RPE. Further, RPE dysfunction led to secondary impairment of choriocapillaris homeostasis. However, it is unknown what domain(s) of Ranbp2 and activities associated to its domains(s) underpin the primary and secondary pathological manifestations of the RPE and choriocapillaris, respectively, caused by loss of *Ranbp2*. This is of critical physiological and therapeutic importance because it will help to uncover targets and mechanisms essential to RPE homeostasis and amenable to pharmacological manipulation in RPE degenerative conditions. To ascertain what domain(s) of Ranbp2 and allied activities are vital to RPE homeostasis, we carried out genetic complementation studies with BACs of *Ranbp2* harboring loss-of-function mutations in distinct domains and expressed these singly in a constitutive *Ranbp2*$^{-/-}$ background (Fig. 5, *A–E*). As described next, the bases for the introduction of loss-of-function mutations in *Ranbp2* domains were built on prior and extensive structure-function analyses of Ranbp2 that showed that such mutations impaired the association of selective domains of Ranbp2 with specific partners. We examined first the following four transgenic (*Tg*) BAC lines of mutant *Ranbp2* in a constitutive *Ranbp2*$^{-/-}$ background: 1) $Tg^{CYm\text{-}HA}$::*Ranbp2*$^{-/-}$ expressing a transgenic *Ranbp2* with loss of PPIase and C-terminal chaperone functions of its cyclophilin (CY) domain (64) in a constitutive *Ranbp2*$^{-/-}$ background; 2) $Tg^{KBDm\text{-}HA}$::*Ranbp2*$^{-/-}$ expressing a transgenic *Ranbp2* with loss of kinesin-1-binding activities in its kinesin-1-binding domain (KBD) (82–85) in a constitutive *Ranbp2*$^{-/-}$ background (Fig. 5*C*); 3) $Tg^{CLDm\text{-}HA}$::*Ranbp2*$^{-/-}$ expressing a transgenic *Ranbp2* with loss of SUMO-1 and S1 (Rpn2)-binding activities in its cyclophilin-like domain (CLD) (64, 80) in a constitutive *Ranbp2*$^{-/-}$ background (Fig. 5*D*); and 4) $Tg^{RBD3*\text{-}HA}$::*Ranbp2*$^{-/-}$ expressing a transgenic *Ranbp2* with loss of Ran-GTP binding of RBD3 of Ranbp2 (50, 85) in a constitutive *Ranbp2*$^{-/-}$ background (Fig. 5*E*).

We found that all four transgenic *Ranbp2* constructs rescued the lethality of *Ranbp2*$^{-/-}$ mice (24, 26), albeit the penetrance of the mutations causing embryonic lethality varied significantly between the transgenic lines. A complete rescue effect was observed with $Tg^{CYm\text{-}HA}$::*Ranbp2*$^{-/-}$ (64). By contrast, the expected progenies from crosses producing $Tg^{KBDm\text{-}HA}$::*Ranbp2*$^{-/-}$, $Tg^{CLDm\text{-}HA}$::*Ranbp2*$^{-/-}$ (64), and $Tg^{RBD3*\text{-}HA}$::*Ranbp2*$^{-/-}$ deviated significantly from the expected Mendelian ratios ($Tg^{KBDm\text{-}HA}$::*Ranbp2*$^{-/-}$: $\chi^2 = 30.0$, $p < 0.0001$; $Tg^{RBD3*\text{-}HA}$::*Ranbp2*$^{-/-}$: $\chi^2 = 54.096$, $p < 2.0 \times 10^{-15}$). The surviving mice did not exhibit overt anatomical and behavioral phenotypes, and all transgenic lines rescued completely the Parkinsonian tremor phenotypes observed in a fraction of *RPE-cre*::*Ranbp2*$^{-/-}$ mice. Importantly, all transgenic *Ranbp2* lines rescued RPE degeneration. No differences in the RPE and permeability of choriocapillaris were found by bright field and fluorescein fundoscopy and morphometric and confocal analyses of the RPE between wild-type, $Tg^{CYm\text{-}HA}$::*Ranbp2*$^{-/-}$, $Tg^{KBDm\text{-}HA}$::*Ranbp2*$^{-/-}$, $Tg^{CLDm\text{-}HA}$::*Ranbp2*$^{-/-}$, and $Tg^{RBD3*\text{-}HA}$::*Ranbp2*$^{-/-}$ mice using the same parameters as those applied to *RPE-cre*::*Ranbp2*$^{-/-}$ (Fig. 5, *C–E*) (data not shown). Hence, the loss of functions of CY, KBD, CLD, and RBD3 modules of Ranbp2 lack untoward physiological effects in RPE and choriocapillaris homeostasis.

Loss of Ran-GTP Binding of RBD2 and RBD3 of Ranbp2 Is Selectively Essential to RPE Survival—In contrast to the previous transgenic *Ranbp2* lines described, progenies expressing $Tg^{RBD2/3*\text{-}HA}$ in a constitutive *Ranbp2*$^{-/-}$ background ($Tg^{RBD2/3*\text{-}HA}$::*Ranbp2*$^{-/-}$) could not be recovered, thus indicating that the loss of Ran-GTP binding of RBD2 and RBD3 of Ranbp2 (50, 85) is essential to mouse viability. Hence, we set out to examine whether the expression of $Tg^{RBD2/3*\text{-}HA}$ (Fig. 6*A*) played differential roles in the rescue of degeneration of two distinct cell types, cone photoreceptor neurons and RPE, where Ranbp2 function(s) are known to play critical roles, as shown by this and other studies (34). We first examined mice, $Tg^{RBD2/3*\text{-}HA}$::*cone-cre*::*Ranbp2*$^{-/-}$, expressing $Tg^{RBD2/3*\text{-}HA}$ in M- and S-cone photoreceptor neurons without endogenous

FIGURE 4. **Confocal images of *en face* RPE of +/+ and −/− mice at P35 showing co-immunostaining of importin-β and Ranbp2 (*A*), exportin-1/Crm1 and Ubc9 (*B*), Ran GTPase and Ranbp2 (*C*), ubiquitin and Ranbp2 (*D*), Stat3 and Stat3(P) (*E*), and ErbB2 counterstained with phalloidin (*F*).** All specimens were counterstained with DAPI. Compared with +/+, localization of importin-β was lacking in nuclei without Ranbp2 (*A*, *arrows*), there were no prominent localization changes in exportin-1/Crm1 in −/− (*B*), there was a decrease of Ran GTPase staining of nuclei (*C*), there was formation of dispersed intracellular puncta and decreased Ubc9 in the nucleus (*B*), there was cytosolic dispersion of ubiquitin (*Ub*) from the nuclear compartment (*D*), there was a loss of plasma membrane localization of Stat3(P) (*E*), and there was relocation of ErbB2 to the nuclear compartment and ErbB2 sequestration in actin clouds (*F*). +/+, *RPE-cre*::*Ranbp2*$^{+/+}$; −/−, *RPE-cre*::*Ranbp2*$^{-/-}$; *scale bars*, 50 μm (*A–F*).

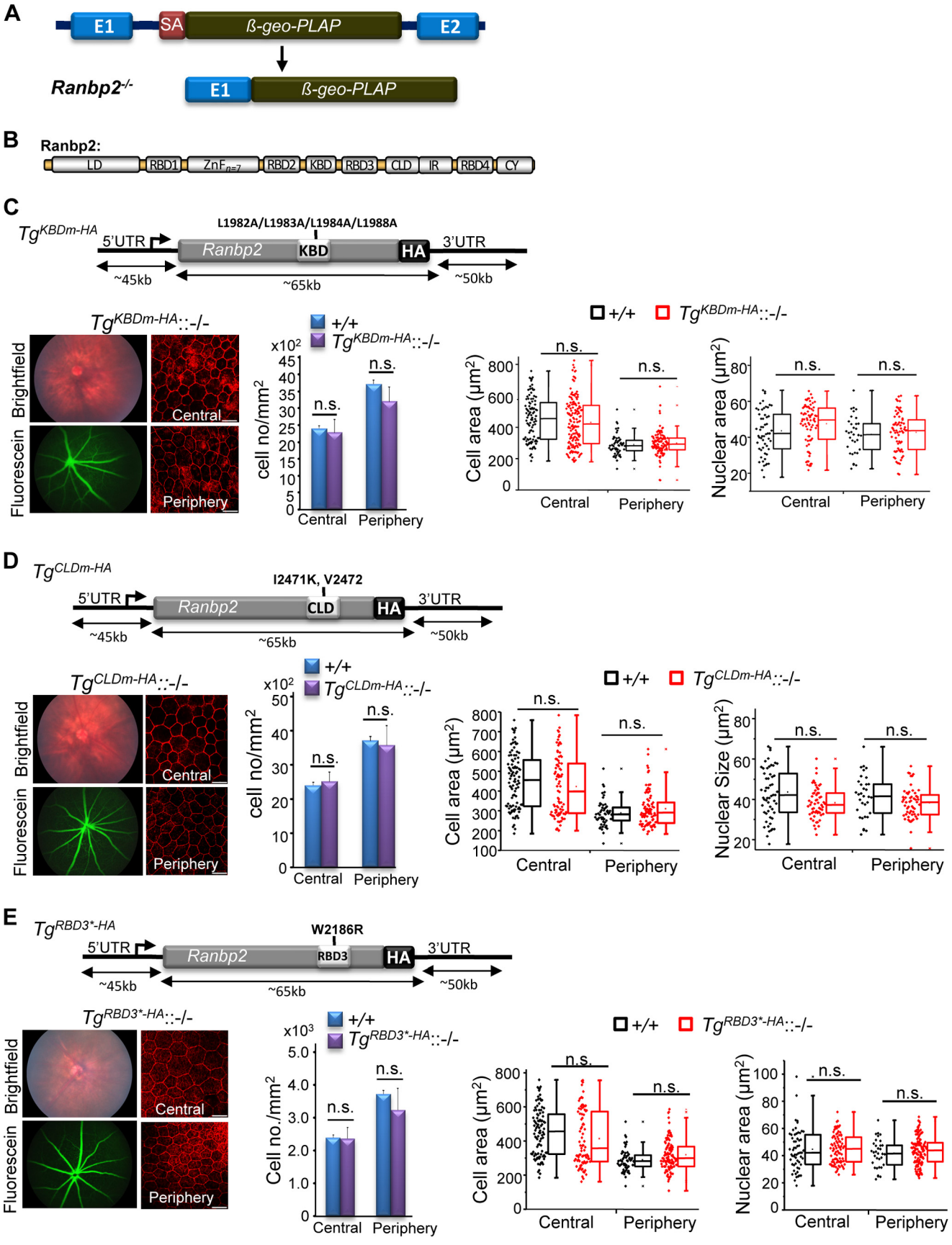
A
E1
SA
ß-geo-PLAP
E2
Ranbp2-/-
E1
ß-geo-PLAP
B
Ranbp2:
LD
RBD1
ZnF n=7
RBD2
KBD
RBD3
CLD
IR
RBD4
CY
C
TgKBDm-HA
L1982A/L1983A/L1984A/L1988A
5'UTR
Ranbp2
KBD
HA
3'UTR
~45kb
~65kb
~50kb
TgKBDm-HA::-/-
Brightfield
Fluorescein
Central
Periphery
+/+
TgKBDm-HA::-/-
x10²
cell no/mm²
n.s.
Central
Periphery
+/+
TgKBDm-HA::-/-
Cell area (µm²)
Nuclear area (µm²)
n.s.
Central
Periphery
D
TgCLDm-HA
I2471K, V2472
5'UTR
Ranbp2
CLD
HA
3'UTR
~45kb
~65kb
~50kb
TgCLDm-HA::-/-
Brightfield
Fluorescein
Central
Periphery
+/+
TgCLDm-HA::-/-
x10²
cell no/mm²
n.s.
Central
Periphery
+/+
TgCLDm-HA::-/-
Cell area (µm²)
Nuclear Size (µm²)
n.s.
Central
Periphery
E
TgRBD3*-HA
W2186R
5'UTR
Ranbp2
RBD3
HA
3'UTR
~45kb
~65kb
~50kb
TgRBD3*-HA::-/-
Brightfield
Fluorescein
Central
Periphery
+/+
TgRBD3*-HA::-/-
x10³
Cell no./mm²
n.s.
Central
Periphery
+/+
TgRBD3*-HA::-/-
Cell area (µm²)
Nuclear area (µm²)
n.s.
Central
Periphery

Ranbp2 (34). $Tg^{RBD2/3*\text{-}HA}$::*cone-cre*::$Ranbp2^{-/-}$ presented partial impairment of M/S-cone development, as shown by a decrease of the number of cone photoreceptors at P20. However, mature M/S-cones in $Tg^{RBD2/3*\text{-}HA}$::*cone-cre*::$Ranbp2^{-/-}$ were rescued from rampant degeneration because their numbers did not decrease between P20 and 12 weeks of age, when retinas are coneless in *cone-cre*::$Ranbp2^{-/-}$ mice (Fig. 6, *B* and *C*) (34). Further, there were no significant differences in the length of outer segments of mature M/S-cones between wild type (*cone-cre*::$Ranbp2^{+/+}$) and $Tg^{RBD2/3*\text{-}HA}$::*cone-cre*::$Ranbp2^{-/-}$ (Fig. 6*D*). Despite the lesser number of cones in $Tg^{RBD2/3*\text{-}HA}$::*cone-cre*::$Ranbp2^{-/-}$, the amplitude of the light-adapted ERGs was rescued in $Tg^{RBD2/3*\text{-}HA}$::*cone-cre*::$Ranbp2^{-/-}$ close to those recorded for wild-type mice (Fig. 6*E*).

Next we examined the effects of $Tg^{RBD2/3*\text{-}HA}$ expression in RPE with an $Ranbp2^{-/-}$ background ($Tg^{RBD2/3*\text{-}HA}$::*RPE-cre*::$Ranbp2^{-/-}$; Fig. 7*A*). Compared with the endogenous Ranbp2 mRNA and protein of wild-type mice, $Tg^{RBD2/3*\text{-}HA}$::*RPE-cre*::$Ranbp2^{-/-}$ presented ~30% transcriptional reduction of $Tg^{RBD2/3*\text{-}HA}$, but the expression of $Tg^{RBD2/3*\text{-}HA}$ protein restored its expression level similar to that of Ranbp2 of wild-type mice (Fig. 7*B*). Confocal microscopy of the RPE of $Tg^{RBD2/3*\text{-}HA}$::*RPE-cre*::$Ranbp2^{-/-}$ showed that the $Tg^{RBD2/3*\text{-}HA}$ protein localized correctly to nuclei of RPE cells (Fig. 7*C*), but bright field and fluorescein fundi of live $Tg^{RBD2/3*\text{-}HA}$::*RPE-cre*::$Ranbp2^{-/-}$ mice showed degeneration of the RPE as early as P14, followed by prominent leakage of the choriocapillaris by P35 (Fig. 7*D*). Confocal microscopy of *en face* fluorescence-labeled phalloidin RPE cells of $Tg^{RBD2/3*\text{-}HA}$::*RPE-cre*::$Ranbp2^{-/-}$ showed that they had prominent hypoplasia and loss of cuboidal architecture and junctional integrity, and these phenotypes appeared more prevalent in the central than in the peripheral regions of the RPE (Fig. 7*E*). We carried out morphometric analyses of the RPE at different ages to characterize in detail the temporal and morphological changes of the RPE of $Tg^{RBD2/3*\text{-}HA}$::*RPE-cre*::$Ranbp2^{-/-}$ mice. The RPE presented an age-dependent increase of hypoplasia (Fig. 7*F*) and cell area (Fig. 7*G*), pathologies that were evident at P14 and more pronounced in the central RPE, but they became significant also in the peripheral region by 24 weeks of age. There was also an increase of the nuclei size of RPE cells that developed earlier in the central than in the peripheral RPE (Fig. 7*H*) and the development of syncytia with up to four nuclei that were also more prominent in the central than in the peripheral RPE (Fig. 7*I*). The RPE of $Tg^{RBD2/3*\text{-}HA}$::*RPE-cre*::$Ranbp2^{-/-}$ showed patches of hyperpigmentation and hypopigmentation (Fig. 7*J*, *top*) and the extrusion of hyperpigmented and atrophic RPE cells into the subretinal space (Fig. 7*J*, *bottom*). In comparison with wild-type mice, these RPE pathologies were accompanied by ~3.5-fold up-regulation of the transcription levels of *Mmp11* in the RPE of $Tg^{RBD2/3*\text{-}HA}$::*RPE-cre*::$Ranbp2^{-/-}$ (Fig. 7*K*). Hence, the RPE cells of $Tg^{RBD2/3*\text{-}HA}$::*RPE-cre*::$Ranbp2^{-/-}$ develop pathologies similar to those of *RPE-cre*::$Ranbp2^{-/-}$ mice, and the pathobiological effects of $Tg^{RBD2/3*\text{-}HA}$ expression are selective to RPE cells.

Shared Mechanisms of RPE Degeneration between RPE-cre::$Ranbp2^{-/-}$ *and* $Tg^{RBD2/3*\text{-}HA}$::*RPE-cre*::$Ranbp2^{-/-}$—The data thus far show that only a subset of pleiotropic activities associated with Ranbp2 functions, such as control of Ran GTPase functions by RBD2 and RBD3, are physiologically relevant to RPE survival. To gain additional insights into what targets and molecular processes are deregulated and shared between *RPE-cre*::$Ranbp2^{-/-}$ and $Tg^{RBD2/3*\text{-}HA}$::*RPE-cre*::$Ranbp2^{-/-}$ mice, we took unbiased and targeted proteomic approaches to screen, identify, and validate proteins with proteostatic changes of RPE homogenates shared between *RPE-cre*::$Ranbp2^{-/-}$ and $Tg^{RBD2/3*\text{-}HA}$::*RPE-cre*::$Ranbp2^{-/-}$ mice but not wild-type *Ranbp2* mice (*RPE-cre*::$Ranbp2^{+/+}$). The approach comprised the screening of proteostatic changes of RPE substrates by 2D-DIGE, mass spectrometry, and targeted immunoscreening of P14 mice (64). Five targets with proteostatic changes in the RPE of *RPE-cre*::$Ranbp2^{-/-}$ and $Tg^{RBD2/3*\text{-}HA}$::*RPE-cre*::$Ranbp2^{-/-}$, but not wild-type mice, were identified and validated. Compared with wild-type mice (*RPE-cre*::$Ranbp2^{+/+}$), the RPE of *RPE-cre*::$Ranbp2^{-/-}$ and $Tg^{RBD2/3*\text{-}HA}$::*RPE-cre*::$Ranbp2^{-/-}$ shared a significant reduction, increase, and reduction, respectively, of Ran GTPase, serotransferrin, and γ-tubulin (Fig. 8, *A*–*C*). Further, there were no transcriptional changes of *Ran GTPase* in any genotype, but there was a transcriptional decrease of serotransferrin selectively in $Tg^{RBD2/3*\text{-}HA}$::*RPE-cre*::$Ranbp2^{-/-}$ and transcriptional reductions of γ-tubulin in *RPE-cre*::$Ranbp2^{-/-}$ and $Tg^{RBD2/3*\text{-}HA}$::*RPE-cre*::$Ranbp2^{-/-}$ (Fig. 8, *A*–*C*). Two other proteostatic changes were also identified in endophilin B1 and Arl2 (ADP-ribosylation factor-like 2 protein), but they were inversely changed (decreased and increased) between *RPE-cre*::$Ranbp2^{-/-}$ and $Tg^{RBD2/3*\text{-}HA}$::*RPE-cre*::$Ranbp2^{-/-}$ (Fig. 8*D*). The selectivity of the $Tg^{RBD2/3*\text{-}HA}$ effects in proteostasis was further examined by assessing the proteostatic levels of other substrates controlled by Ranbp2 or selectively by other domains of Ranbp2 (64, 79, 80). We observed that the levels of Rpe65, Stat3, exportin-1/Crm1, S1 (Rpn2) subunit of the 26 S proteasome, and sumoylated RanGAP were exclusively reduced in *RPE-cre*::$Ranbp2^{-/-}$ (Fig. 8*E*). Collectively, these data support that loss of *Ranbp2* elicits a broad impairment in

FIGURE 5. **Transgenic BAC constructs of *Ranbp2* with loss-of-function mutations in KBD ($Tg^{KBDm\text{-}HA}$), CLD ($Tg^{CLDm\text{-}HA}$), or RBD3 ($Tg^{RBD3*\text{-}HA}$) expressed in mice with a $Ranbp2^{-/-}$ background (−/−) rescue RPE degeneration and mouse viability.** *A*, constitutive disruption of *Ranbp2* gene expression by the genomic insertion of a promoterless bicistronic (*β-geo-PLAP*) cassette with a splicing acceptor site (*SA*) between exons 1 and 2 leads to the splicing of exon 1 with the terminal bicistronic cassette. *B*, modular structure (domains) of Ranbp2. Selective mutations were introduced in various domains of Ranbp2 as shown in *C*–*E*. $Tg^{KBDm\text{-}HA}$::−/− (*C*), $Tg^{CLDm\text{-}HA}$::−/− (*D*), and $Tg^{RBD3*\text{-}HA}$::−/− mice (*E*) with expression of $Tg^{KBDm\text{-}HA}$, $Tg^{CLDm\text{-}HA}$, and $Tg^{RBD3*\text{-}HA}$, respectively, in a $Ranbp2^{-/-}$ (−/−) background have ordinary fundus and FITC-dextran angiograms, cell densities, and cellular and nuclear areas in the central and peripheral regions of the RPE at P35. The $Tg^{KBDm\text{-}HA}$, $Tg^{CLDm\text{-}HA}$, and $Tg^{RBD3*\text{-}HA}$ constructs of Ranbp2 harbor the mutations L1982A/L1983A/L1984A/L1988A, I2471K/V2472, and W2186R, respectively. $Tg^{KBDm\text{-}HA}$::−/−, $Tg^{KBDm\text{-}HA}$::$Ranbp2^{-/-}$; $Tg^{CLDm\text{-}HA}$::−/−, $Tg^{CLDm\text{-}HA}$::$Ranbp2^{-/-}$; $Tg^{RBD3*\text{-}HA}$::−/−, $Tg^{RBD3*\text{-}HA}$::$Ranbp2^{-/-}$; +/+, $Ranbp2^{+/+}$. Data represent the mean ± S.D. (*error bars*) (cell density); dot-box plot analyses are shown for cellular and nuclear areas. Statistical analysis was done using a Mann-Whitney *U* test at a significance level of 0.05; $n = 3$, $Tg^{KBDm\text{-}HA}$::−/− and $Tg^{CLDm\text{-}HA}$::−/−; $n = 4$, $Tg^{RBD3*\text{-}HA}$::−/−; *n.s.*, non-significant; *LD*, leucine-rich domain; $RBD_{n=1-4}$, Ran GTPase-binding domains, $n = 1$–4; $ZnF_{n=7}$, zinc finger-rich domains; *IR1* + *2*, internal repeat. *Scale bars*, 20 μm (*C*–*E*).

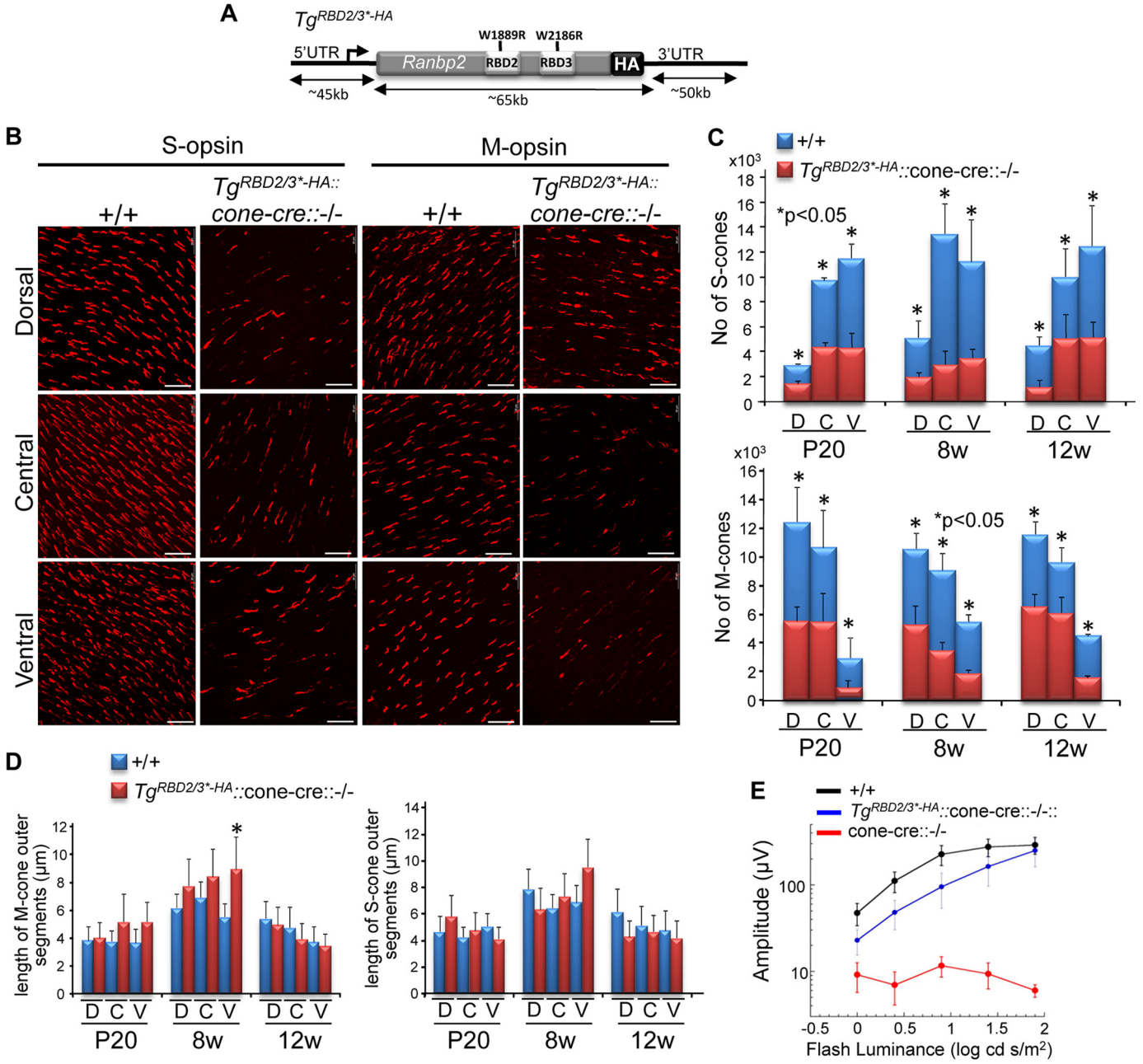

FIGURE 6. **A transgenic BAC construct of *Ranbp2* with Ran-GTP-binding mutations in RBD2 and RBD3 of Ranbp2 (*Tg*$^{RBD2/3*-HA}$) expressed in cone photoreceptors with endogenous ablation of *Ranbp2* (*cone-cre*::−/−) rescues the degeneration of mature S-cone and M-cone photoreceptors.** Retinas of mice with expression of *Tg*$^{RBD2/3*-HA}$ (*A*) in *cone-cre*::*Ranbp2*$^{-/-}$ (*Tg*$^{RBD2/3*-HA}$::−/−) present a reduction of mature S-cones and M-cones in comparison with wild-type mice (+/+), but the mature cone photoreceptors do not undergo degeneration with aging (*B* and *C*). There are also no overall significant changes in the length of the outer segment of mature S-cones and M-cones between +/+ and *Tg*$^{RBD2/3*-HA}$::−/− at different ages (*, $p < 0.05$; all others $p > 0.05$) (*D*). Although slightly underdeveloped compared with wild-type mice (+/+), the light-adapted ERG of *Tg*$^{RBD2/3*-HA}$::−/− is significantly rescued compared with age-matched mice with endogenous ablation of *Ranbp2* in cones (*cone-cre*::−/−) and lacking light-adapted ERG at P29 (E). Data represent the mean ± S.D. (*error bars*), $n = 3–4$ (*C* and *D*) and mean ± S.E. (*error bars*), $n = 4–9$, $p < 0.005$ (−/− *versus* *Tg*$^{RBD2/3*-HA}$::−/−) (*E*); +/+, *cone-cre*::*Ranbp2*$^{+/+}$; −/−, *cone-cre*::*Ranbp2*$^{-/-}$; *Tg*$^{RBD2/3*-HA}$::−/−, *Tg*$^{RBD2/3*-HA}$::*RPE-cre*::*Ranbp2*$^{-/-}$. *Scale bars*, 20 μm (*B*).

proteostasis of RPE proteins controlled by Ranbp2 and that proteostatic impairment of a restricted subset of these proteins by selective loss of function of RBD2 and RBD3 of Ranbp2 suffices to promote RPE degeneration.

In light of the shared and strong down-regulation of Ran GTPase proteostasis in RPE of *RPE-cre*::*Ranbp2*$^{-/-}$ and *Tg*$^{RBD2/3*-HA}$::*RPE-cre*::*Ranbp2*$^{-/-}$ mice, we characterized further biochemical impairments of Ran GTPase between genotypes. First, we examined disturbances in the ratio of Ran-GTP to Ran-GDP and nucleotide-free Ran GTPase between non-transgenic and transgenic lines. In comparison with *RPE-cre*::*Ranbp2*$^{+/+}$, there was a trend for reduced levels of Ran-GTP in *RPE-cre*::*Ranbp2*$^{-/-}$, but such change became significant in *Tg*$^{RBD2/3*-HA}$::*RPE-cre*::*Ranbp2*$^{-/-}$ (Fig. 8*F*). Then we assessed changes in subcellular partitioning of Ran GTPase between the nuclear and non-nuclear (all other) subcellular fractions. As shown in Fig. 8*G*, the small fraction of Ran GTPase retained in the nuclear fraction of RPE of wild-type mice was

released to the non-nuclear fraction of *RPE-cre*::*Ranbp2*$^{-/-}$ and *Tg*$^{RBD2/3*-HA}$::*RPE-cre*::*Ranbp2*$^{-/-}$ mice upon fractionation.

RPE-cre::*Ranbp2*$^{-/-}$ *and Tg*$^{RBD2/3*-HA}$::*RPE-cre*::*Ranbp2*$^{-/-}$ *Present Suppression of Electrophysiological Functions of the RPE*—We used dc-ERGs to measure RPE function *in vivo*. In comparison with *RPE-cre*::*Ranbp2*$^{+/+}$ littermates, the overall amplitude of the dc-ERG was strongly reduced in P35 old *RPE-cre*::*Ranbp2*$^{-/-}$ and *Tg*$^{RBD2/3*-HA}$::*RPE-cre*::*Ranbp2*$^{-/-}$ mice (Fig. 9, *A*–*C*). When the individual waveform components of the dc-ERG were measured, all were significantly reduced in amplitude in *RPE-cre*::*Ranbp2*$^{-/-}$ and *Tg*$^{RBD2/3*-HA}$::*RPE-cre*::*Ranbp2*$^{-/-}$, and the magnitude of the reduction was

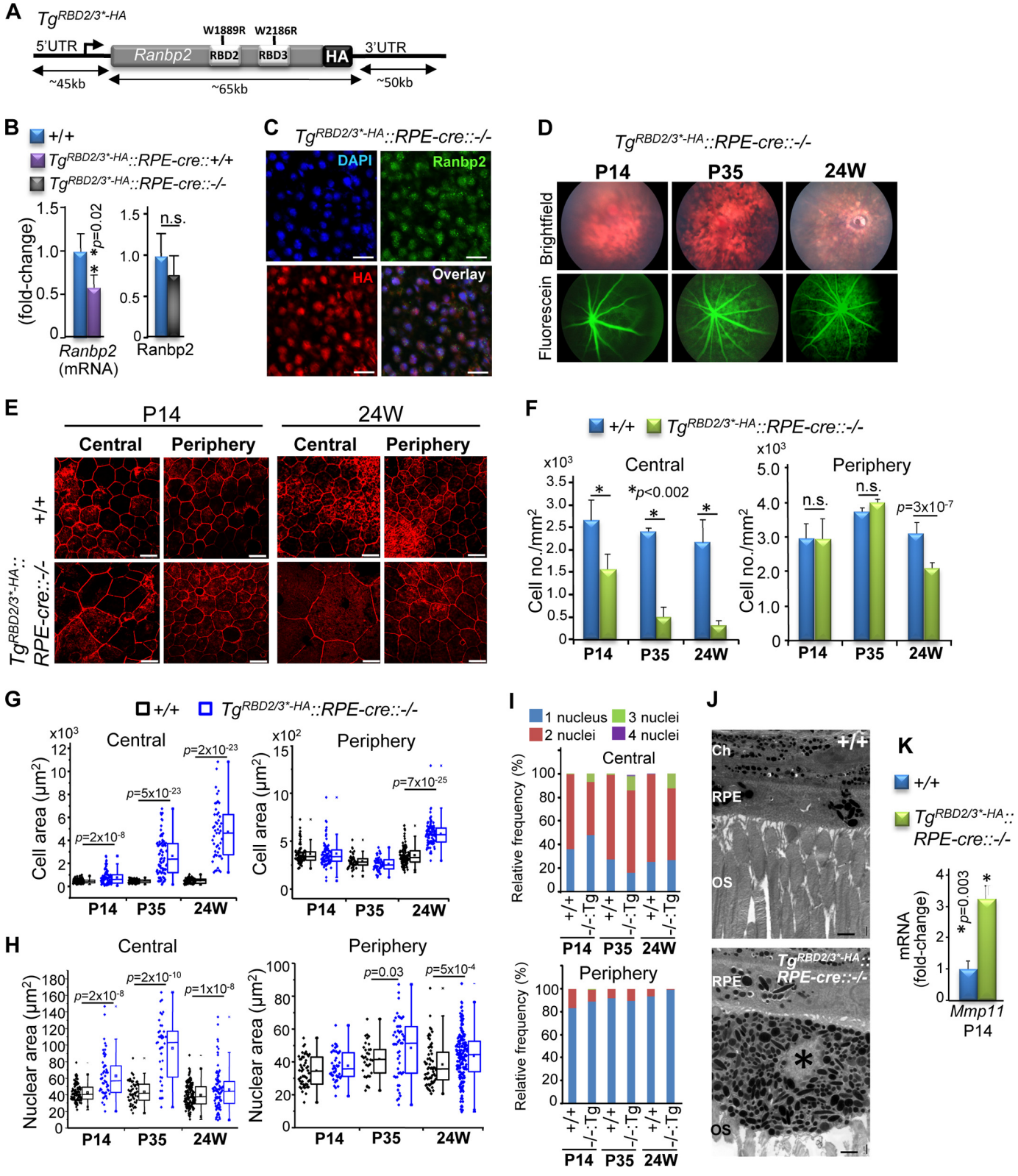

greater in $Tg^{RBD2/3*\text{-}HA}$::*RPE-cre*::$Ranbp2^{-/-}$ (Fig. 9*B*). The dc-ERGs of older mice were also reduced, but the magnitude of the reduction did not change with age (Fig. 9*C*). The exacerbating effect of $Tg^{RBD2/3*\text{-}HA}$::*RPE-cre*::$Ranbp2^{-/-}$ on dc-ERG amplitudes was not due to the transgene itself or a dominant effect of the transgene because the expression of $Tg^{RBD2/3*\text{-}HA}$ in a wild-type RPE background had normal dc-ERG responses (data not shown). Because the dc-ERG is generated secondary to activities of rod photoreceptor neurons (66), the amplitude reduction could reflect a change in RPE function or in the response of the outer retina (86). To examine these possibilities, we recorded strobe flash ERGs at the same ages. The *a*- and *b*-wave amplitudes of dark-adapted and light-adapted ERGs between *RPE-cre*::$Ranbp2^{+/+}$ and *RPE-cre*::$Ranbp2^{-/-}$ mice were not significantly different at P35 (Fig. 9, *D* and *E*). This indicates that the dc-ERG reductions noted at this age do not reflect a reduction in rod photoreceptor activity. However, we found a small but significant reduction of the *a*-wave amplitudes of dark-adapted ERGs of $Tg^{RBD2/3*\text{-}HA}$::*RPE-cre*::$Ranbp2^{-/-}$ compared with *RPE-cre*::$Ranbp2^{+/+}$. ERG *a*- and *b*-waves were significantly reduced in *RPE-cre*::$Ranbp2^{-/-}$ mice at the older ages, an effect that was also accompanied by a significant reduction of the light-adapted ERG (data not shown), indicating an onset of rod and cone photoreceptor dysfunction that was secondary to and later than that for the RPE.

DISCUSSION

The findings of this study establish a critical role of Ranbp2 and selective Ran-GTP binding domains of Ranbp2 in the function and survival of the RPE. The study unveils unique physiological features of Ranbp2 and mechanisms underpinning RPE degeneration. This study demonstrates the following. 1) Ranbp2 and a subset of activities determined by selective structural/functional modules of Ranbp2 exert physiological and vital discriminating roles between cell types (*e.g.* RPE *versus* cones). 2) The RBD1 and RBD4 of Ranbp2, and Ranbp1 cannot compensate physiologically in the RPE for the losses of function of RBD2 and RBD3 of Ranbp2, even though RBD1–4 of Ranbp2 and Ranbp1 are structurally and biochemically equivalent (43, 50); thus, this finding indicates that the functions of RBD2 and RBD3 are spatially constrained within Ranbp2 and probably dependent on their neighboring domains. 3) RPE degeneration caused by chimeric loss of *Ranbp2* and functions of its RBD2 and RBD3 presents centrifugal progression, and this degeneration is compensated by an increase of the proliferative capacity of peripheral RPE. 4) RPE degeneration undergoes atypical cell death mechanisms without activation of caspases and apoptosis but with up-regulation of Mmp11 expression and activity. 5) Chimeric loss of Ranbp2 expression in RPE elicits widespread pathological manifestations across the RPE and choriocapillaris. These observations consolidate the notion that loss of Ranbp2 functions triggers non-autonomous pathological effects in neighboring healthy cells and/or tissues like those observed previously between damaged cones and healthy rods (34). 6) Ranbp2-dependent up-regulation of Mmp11 is controlled by Ran GTPase via RBD2 and RBD3 of Ranbp2, and Mmp11 activation may underpin non-autonomous pathological manifestations allied to RPE degeneration by the destabilization of homotypical and heterotypical cellular architectures and vascular permeability, events that are critical to disease progression. 7) The incomplete penetrance of juvenile Parkinsonian manifestations by *RPE-cre*::$Ranbp2^{-/-}$ and lack of such manifestations by $Tg^{RBD2/3*\text{-}HA}$::*RPE-cre*::$Ranbp2^{-/-}$ and all other transgenic lines described herein indicate that Ranbp2 and genetic modifiers affecting partners to other domains of Ranbp2 control Parkinsonian expression.

A Ran-GTP to Ran-GDP gradient along the mitotic spindle drives bipolar spindle assembly in mitotic cells, whereas nuclear-cytoplasmic trafficking of substrates in interphase cells is thought to be driven by a Ran-GTP to Ran-GDP gradient between the nucleus and the cytosol, respectively (51–57). Ranbp1 and the RBDs of Ranbp2 are the only known high affinity ligands toward Ran-GTP, and they are required to co-stimulate Ran GTPase activity (43, 49, 50, 85). Computational models with Ran GTPase cycle components, but without the inclusion of Ranbp2, predict that the vital maintenance of the Ran nucleotide-bound gradient between cellular compartments is robust and can tolerate fluctuations of factors regulating Ran GTPase activity (45, 46), a prediction that appears to be supported by the constitutive ablation of *Ranbp1* in a mouse model in which organismal viability and cell survival are not affected (47). By contrast, other findings suggest that experimental disturbances of the Ran-GTP gradient promote mitotic catastrophe and collapse of the bidirectional nucleocytoplasmic flux (51, 52). Past studies suggested that Ranbp2 does not play an essential role in nucleocytoplasmic transport (26, 62), but recent studies with cell cultures suggest that distinct RBDs

FIGURE 7. **Transgenic expression of a BAC construct of *Ranbp2* with Ran-GTP-binding mutations in RBD2 and RBD3 of Ranbp2 ($Tg^{RBD2/3*\text{-}HA}$) in RPE with endogenous ablation of *Ranbp2* (*RPE-cre*::−/−) promotes RPE degeneration.** *A*, diagram of $Tg^{RBD2/3*\text{-}HA}$ BAC construct. *B*, the transcriptional expression levels in the RPE of $Tg^{RBD2/3*\text{-}HA}$ allele are reduced by ~30% compared with the endogenous *Ranbp2* levels (*left graph*), but $Tg^{RBD2/3*\text{-}HA}$::*RPE-cre*::−/− and wild-type mice (+/+) present comparable transgenic and endogenous Ranbp2 protein levels (*right graph*), respectively, at P14. *C*, confocal microscopy images of $Tg^{RBD2/3*\text{-}HA}$ protein localization to nuclei of RPE cells of $Tg^{RBD2/3*\text{-}HA}$::*RPE-cre*::−/− with antibodies against HA tag and Ranbp2. *D*, bright field fundoscopy and FITC-labeled dextran angiograms of $Tg^{RBD2/3*\text{-}HA}$::*RPE-cre*::−/− at P14, P35, and 24 weeks of age showing RPE degeneration at all ages and extravasations of FITC-dextran from the choriocapillaris beginning at P35. *E*, *en face* confocal microscopy images of phalloidin-stained RPE showing the degeneration of RPE at P14 and 24 weeks of age in $Tg^{RBD2/3*\text{-}HA}$::*RPE-cre*::−/−. The severity of RPE degeneration is age-dependent and characterized by hypoplasia, atrophic RPE cells, and derangement of the tessellated organization of the RPE and is most severe in the central RPE. Shown are morphometric analyses of RPE showing a decrease of cell density (*F*), increase of cellular (*G*) and nuclear areas (*H*), and an increase of frequency of multinucleation (*I*) of central and peripheral RPE between $Tg^{RBD2/3*\text{-}HA}$::*RPE-cre*::−/− and wild-type mice (+/+) at different ages. *J*, ultrastructural images of radial sections of choroid/RPE and outer segments (*OS*) of photoreceptors of P35 $Tg^{RBD2/3*\text{-}HA}$::*RPE-cre*::−/− showing regions with and without pigmentation of RPE and the escape of a hyperpigmented and atrophic RPE cell into the subretinal space. *K*, compared with +/+ mice, there is a >3-fold increase of the up-regulation of *Mmp11* in $Tg^{RBD2/3*\text{-}HA}$::*RPE-cre*::−/−. Data shown represent the mean ± S.D. (*error bars*), $n = 4$ (*B*, *F*, and *K*); dot-box plot analyses are shown for cell and nuclear areas (*G* and *I*). Statistical analysis was done using a Mann-Whitney *U* test at a significance level of 0.05; $n = 4$ (P14), $n = 5$ (P35), $n = 3$ (24 weeks); *n.s.*, non-significant; +/+, *RPE-cre*::$Ranbp2^{+/+}$; −/−, *RPE-cre*::$Ranbp2^{-/-}$; $Tg^{RBD2/3*\text{-}HA}$::*RPE-cre*::−/−, $Tg^{RBD2/3*\text{-}HA}$::*RPE-cre*::$Ranbp2^{-/-}$; *Tg*:−/−, $Tg^{RBD2/3*\text{-}HA}$::*RPE-cre*::$Ranbp2^{-/-}$ (*I*); *scale bars*, 20 μm (*C* and *E*), 2 μm (*J*); *OS*, outer segments; *Ch*, choroid; *, atrophic RPE cell in subretinal space.

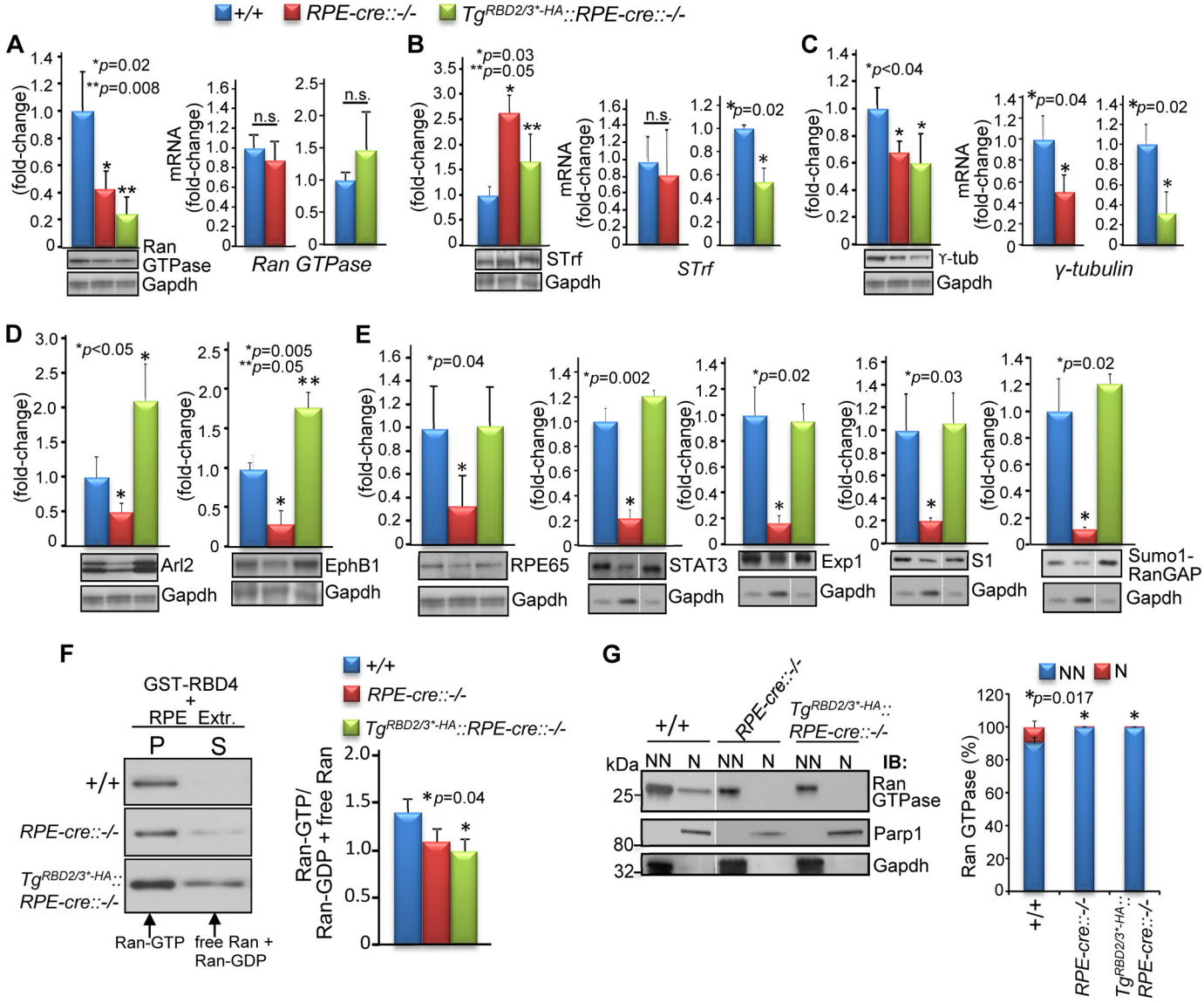

FIGURE 8. **Shared and unique changes in proteostasis of RPE at P14 between wild-type mice (+/+), mice with endogenous ablation of *Ranbp2* in the RPE (*RPE-cre*::−/−), and mice expressing $Tg^{RBD2/3*-HA}$ in RPE with endogenous ablation of *Ranbp2* ($Tg^{RBD2/3*-HA}$::*RPE-cre*::−/−).** In comparison with +/+, the Ran GTPase (*A*) and serotransferrin protein (*B*) levels are decreased and increased, respectively, without a change of their transcriptional levels in *RPE-cre*::−/− and $Tg^{RBD2/3*-HA}$::*RPE-cre*::−/−, with the exception of a compensatory transcriptional decrease of serotransferrin in $Tg^{RBD2/3*-HA}$::*RPE-cre*::−/−. *C*, *RPE-cre*::−/− and $Tg^{RBD2/3*-HA}$::*RPE-cre*::−/− compared with +/+ mice have a decrease of protein and mRNA levels of γ-tubulin. *D*, in comparison with +/+ mice, Arl2 and endophilin B1 (*EphB1*) are decreased and increased in the *RPE-cre*::−/− and $Tg^{RBD2/3*-HA}$::*RPE-cre*::−/−, respectively. *E*, the proteostatic levels of Rpe65, Stat3, exportin-1/Crm1 (*Exp1*), S1 subunit (*Rpn2*) of the 19 S cap of the proteasome, and SUMO-1-RanGAP are decreased selectively in *RPE-cre*::−/− but not $Tg^{RBD2/3*-HA}$::*RPE-cre*::−/− and +/+ mice. *F*, immunoblots of Ran GTPase from coprecipitates (*P*) and supernatants (*S*) of pull-down assays with GST-RBD4 of RPE-solubilized Nonidet P-40 extracts of +/+, *RPE-cre*::−/−, and $Tg^{RBD2/3*-HA}$::*RPE-cre*::−/− mice (representative immunoblot on the *left*) and quantitative analyses of ratios of Ran-GTP to Ran-GDP and nucleotide free Ran (graph on the *right*). *G*, changes in subcellular partitioning of Ran GTPase between nuclear (*N*) and non-nuclear (*NN*) fractions of RPE between +/+, *RPE-cre*::−/−, and $Tg^{RBD2/3*-HA}$::*RPE-cre*::−/− mice. Parp1 and Gadph are nuclear and cytosolic markers, respectively. Representative immunoblots and loading controls are shown *below* the graphs in *A*–*F*. Data shown represent the mean ± S.D. (*error bars*), $n = 4$; *n.s.*, non-significant; +/+, *RPE-cre*::*Ranbp2*$^{+/+}$; *RPE-cre*::−/−, *RPE-cre*::*Ranbp2*$^{-/-}$; $Tg^{RBD2/3*-HA}$::*RPE-cre*::−/−, $Tg^{RBD2/3*-HA}$::*RPE-cre*::*Ranbp2*$^{-/-}$; *STrf*, serotransferrin; *exp1*, exportin-1; *S1*, S1(Rpn2) subunit of the 26 S proteasome; *Parp1*, poly(ADP-ribose) polymerase 1; *Gadph*, glyceraldehyde 3-phosphate dehydrogenase.

and regions of Ranbp2 play cell type- or substrate-dependent roles in supporting nuclear-cytoplasmic trafficking and cellular viability (60, 61). Regardless, the physiological role(s) of any RBD of Ranbp2 remains heretofore elusive. Unexpectedly, our results indicate that the regulation of Ran GTPase by only a subset of presumably redundant RBDs of Ranbp2 is vital to selective cell types, such as RPE, but not mature cone photoreceptor neurons and that *Ranbp2* and its RBDs are dispensable for mitotic progression/proliferation of peripheral RPE cells in response to degeneration of the central RPE. These findings are apparently at odds with cell culture studies of Ranbp2, where Ranbp2 was required for mitosis (58, 59), and the N-terminal leucine-rich domain together with its neighboring RBD1 sufficed to support cell growth and survival and nucleocytoplasmic transport of classical nuclear localization signal-mediated protein import of non-physiological reporter substrates without impairment of M9-mediated protein import and exportin-1/Crm1-mediated protein and mRNA export (60). Regardless, these apparent discrepancies are probably reconciled by the selective roles of Ranbp2, its RBDs, or other domains in the

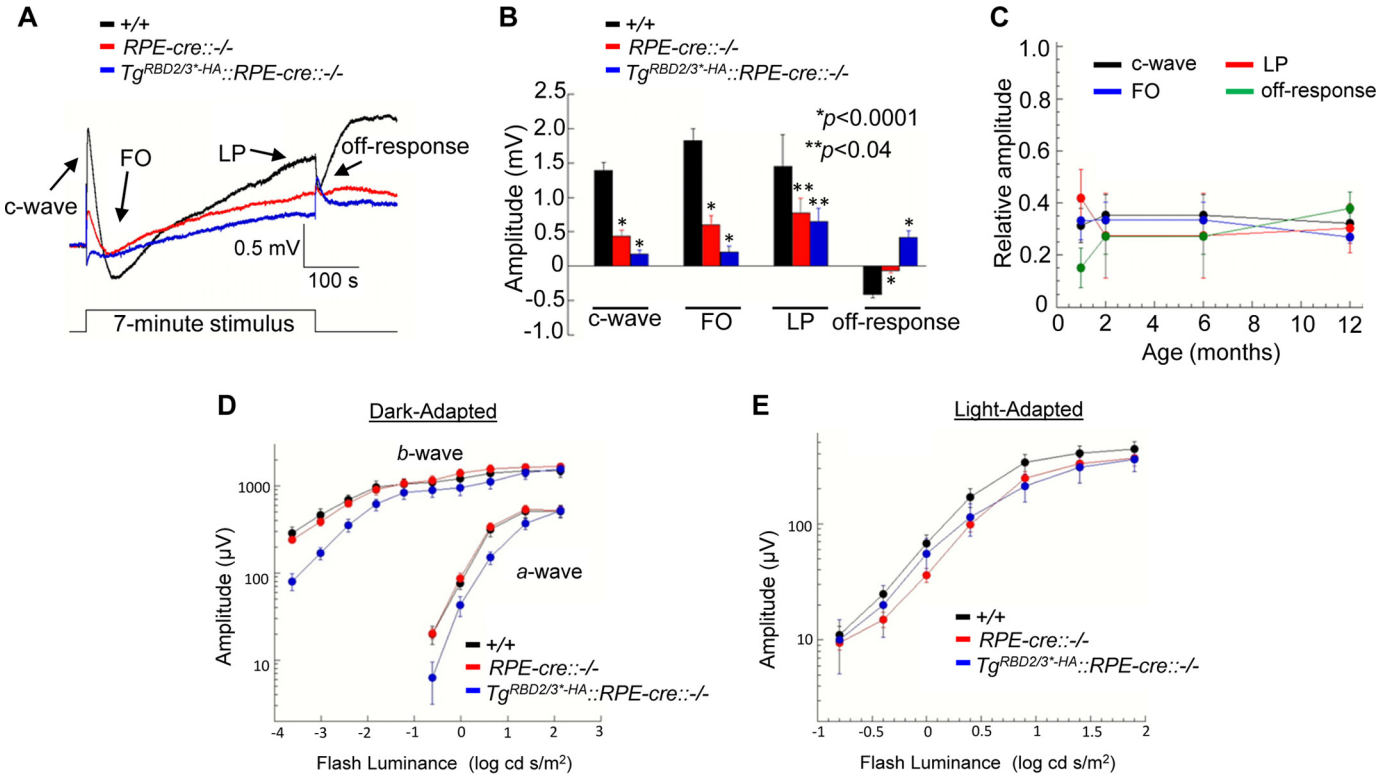

FIGURE 9. **Electrophysiological responses of RPE and outer retina.** *A*, average dc-ERGs obtained to a 7-min duration 2.4 log cd/m^2 stimulus from wild-type (+/+), *RPE-cre*::−/−, and $Tg^{RBD2/3*\text{-}HA}$::*RPE-cre*::−/− mice at P35. *B*, amplitudes of the major dc-ERG components measured in +/+, *RPE-cre*::−/−, and $Tg^{RBD2/3*\text{-}HA}$::*RPE-cre*::−/− littermates at P35. In comparison with +/+, dc-ERG amplitudes are suppressed in *RPE-cre*::−/− and $Tg^{RBD2/3*\text{-}HA}$::*RPE-cre*::−/− ($p <$ 0.0001 for *c*-wave, FO, and off-response; $p < 0.04$ for light peak (*LP*)). *C*, the amplitude reduction of the dc-ERG remains stable in older *RPE-cre*::−/−. For each component, the amplitudes of the *RPE-cre*::−/− responses are expressed relative to those of +/+ littermates. *D* and *E*, outer retinal function measured with strobe flash ERG. Shown are luminance-response functions for the major components of the dark-adapted (*D*) and light-adapted (*E*) ERGs obtained from +/+, *RPE-cre*::−/−, and $Tg^{RBD2/3*\text{-}HA}$::*RPE-cre*::−/− littermates at P35. The *a*- and *b*-wave amplitudes of dark-adapted and light-adapted ERGs between +/+ and *RPE-cre*::−/− mice were not significantly different, but there was a small but significant reduction of the *a*-wave amplitude of dark-adapted ERGs of $Tg^{RBD2/3*\text{-}HA}$::*RPE-cre*::−/− compared with +/+ ($p < 0.004$). Data shown represent the mean ± S.E. (*error bars*), $n = 6$–11 (*B* and *C*) and $n = 7$–18 (*D* and *E*). +/+, *RPE-cre*::$Ranbp2^{+/+}$; *RPE-cre*::−/−, *RPE-cre*::$Ranbp2^{-/-}$; $Tg^{RBD2/3*\text{-}HA}$::*RPE-cre*::−/−, $Tg^{RBD2/3*\text{-}HA}$::*RPE-cre*::$Ranbp2^{-/-}$.

regulation of cell type-restricted substrates impinging on distinct facets of cellular viability and function. In this regard, our findings uncover a number of physiological substrates in the RPE, such as Ran GTPase, Mmp11, Rpe65, Ubc9, ubiquitin, ErbB2, Stat3, exportin-1/Crm1, S1 subunit of the proteasome, γ-tubulin, SUMO-1 RanGAP, serotransferrin, Arl2, and endophilin B1, whose proteostasis and/or subcellular localizations are controlled by Ranbp2 (*RPE-cre*::$Ranbp2^{-/-}$), whereas the homeostasis of a subset of these substrates, such as Ran GTPase, Mmp11, serotransferrin, Arl2, and endophilin B1, are uniquely controlled by RBD2 and RBD3 of Ranbp2 ($Tg^{RBD2/3*\text{-}HA}$::*RPE-cre*::$Ranbp2^{-/-}$), and their proteostatic impairments suffice to promote RPE degeneration. Follow-up studies are needed to determine the precise individual and interdependent contribution(s) of these substrates to the onset and progression of primary and secondary (*e.g.* choriocapillaris) pathologies of the RPE.

Another important finding of this study was that *RPE-cre*::$Ranbp2^{-/-}$ and $Tg^{RBD2/3*\text{-}HA}$::*RPE-cre*::$Ranbp2^{-/-}$ mice shared the centrifugal progression of degeneration of the RPE. It is thought that the central RPE becomes senescent due to hyperplastic senile changes first proposed by Duke-Elder and Perkins (87), whereas the peripheral RPE retains repair capacity due to its competency to reenter the cell cycle (70). Although the molecular bases for the proliferative capacity of peripheral RPE are unresolved, they may arise from emmetropization, a coordinated process of development and growth of various tissues of the eye by mechanisms not yet elucidated (70, 88). Interestingly, a recent study showed that down-regulation of Ran GTPase promotes cellular senescence possibly by decreasing competency of nucleocytoplasmic transport driven by Ran GTPase (89). Our findings of the down-regulation of proteostasis and impairment of subcellular partitioning of Ran GTPase in *RPE-cre*::$Ranbp2^{-/-}$ and $Tg^{RBD2/3*\text{-}HA}$::*RPE-cre*::$Ranbp2^{-/-}$ mice suggest that Ran GTPase deficits play an important role in triggering or augmenting senescent-like manifestations of a preordained region of the RPE to age-dependent degeneration.

Interestingly, Arl2 and endophilin B1 are differentially deregulated between *RPE-cre*::$Ranbp2^{-/-}$ and $Tg^{RBD2/3*\text{-}HA}$::*RPE-cre*::$Ranbp2^{-/-}$. Compared with *RPE-cre*::$Ranbp2^{-/-}$, the deficits of all waveform components of dc-ERG were exacerbated in $Tg^{RBD2/3*\text{-}HA}$::*RPE-cre*::$Ranbp2^{-/-}$, whereas the secondary effects on deficits of the dark-adapted ERG of rod photoreceptors appeared first in this transgenic line. Hence, the distinct deregulations of Arl2 and endophilin B1 between the genotypes may contribute to differential changes in waveform components of dc-ERG observed between the lines. The absence of rod ERG deficits of *RPE-cre*::$Ranbp2^{-/-}$ is surprising because ablation of *Ranbp2* caused the down-regulation of visual cycle

components of the RPE, such as Rpe65, which is required to restore the levels of the chromophore, 11-*cis*-retinal, in phototransduction. It is possible that the existence of an alternative visual cycle in Müller cells (90) compensates for the Ranbp2-mediated down-modulation of visual cycle components of the RPE, but this issue requires further investigation.

Finally, we have shown previously that ablation of *Ranbp2* in cones promotes the necrotic death of cones and non-autonomous apoptosis of healthy rods by atypical cell death mechanisms that involve the temporal activation of distinct caspases (34). By contrast, the mechanism(s) underlying the death of RPE cells in diseases causing RPE degeneration are poorly understood. In particular, it is still unclear whether activation of caspases plays a role in RPE degeneration because some studies implicate caspase-1, -3, and -8 in RPE cell death (91, 92), whereas others found no evidence of activation of caspase-3, -7, and -9 and apoptosis (93). Our findings show that ablation of *Ranbp2* in the RPE promotes its degeneration by neither caspase activation nor apoptotic cell death. Hence, it is likely that multiple insults to the RPE elicit the activation of distinct cell death pathways in the RPE. Regardless, the activation of Mmp11 by cones (34) and RPE cells upon ablation of *Ranbp2* cements its status as a central player in cone and RPE degeneration, and Mmp11 secretion to the extracellular matrix by damaged cells may also underpin non-autonomous pathological processes in neighboring healthy cells and tissues. We propose that this mechanism contributes markedly to the loss of permeability of the choriocapillaris and the extrusion of atrophic RPE cells to the subretinal space during RPE degeneration. Interestingly, extrusion of atrophic RPE cells to the subretinal space has been reported in other mouse models of RPE degeneration (93, 94); thus, this trait probably reflects a broad pathological manifestation resulting from RPE cell death. Further, the Ranbp2-dependent activation of Mmp11 may be co-opted by etiologically distinct diseases, such as carcinogenesis, where breakdown of cellular architecture and cellular intravasation and extravasation by deregulation of vascular homeostasis are central to disease progression (95, 96).

In summary, this study uncovers novel Ranbp2-dependent mechanisms and targets promoting RPE degeneration with secondary pathological effects on neighboring tissues that, in aggregate, are critical to chorioretinal homeostasis. These findings will aid in the development of pharmacological approaches with therapeutic potential in diseases, such as age-related macular degeneration, where the functions and survival of the RPE and other neighboring tissues and the orchestration of nuclear-cytoplasmic flow and/or proteostasis of selective substrates are compromised.

Acknowledgments—We thank Jason Luo for help with the morphometric analyses of cone photoreceptors; Nomingerel Tserentsoodol for help with the capturing of a few confocal images; J. M. van Deursen (Mayo Clinic) for the floxed Ranbp2; Yun-Zheng Le (University of Oklahoma Health Sciences Center) for the RPE-cre and cre-HRGP mice; Neal Copeland (Methodist Hospital Research Institute, formerly at NCI, National Institutes of Health) for the BAC recombineering vectors and protocols; and Cheryl Bock (Transgenic Mouse Facility) and Ute Hochgeschwender (Duke Neurotransgenic Laboratory, Duke University Medical Center) for the microinjections of BAC constructs into one-cell fertilized mouse embryos.

REFERENCES

1. Bok, D. (1993) The retinal pigment epithelium: a versatile partner in vision. *J. Cell Sci. Suppl.* **17,** 189–195
2. Strauss, O. (2005) The retinal pigment epithelium in visual function. *Physiol. Rev.* **85,** 845–881
3. Marmor, M. F., and Wolfensberger, T. J. (1998) *The Retinal Pigment Epithelium: Current Aspects of Function and Disease*, Oxford University Press, New York
4. Rattner, A., and Nathans, J. (2006) Macular degeneration: recent advances and therapeutic opportunities. *Nat. Rev. Neurosci.* **7,** 860–872
5. Jager, R. D., Mieler, W. F., and Miller, J. W. (2008) Age-related macular degeneration. *N. Engl. J. Med.* **358,** 2606–2617
6. Bird, A. C., Bressler, N. M., Bressler, S. B., Chisholm, I. H., Coscas, G., Davis, M. D., de Jong, P. T., Klaver, C. C., Klein, B. E., and Klein, R. (1995) An international classification and grading system for age-related maculopathy and age-related macular degeneration. The International ARM Epidemiological Study Group. *Surv. Ophthalmol.* **39,** 367–374
7. Marmorstein, A. D., Cross, H. E., and Peachey, N. S. (2009) Functional roles of bestrophins in ocular epithelia. *Prog. Retin. Eye Res.* **28,** 206–226
8. Maw, M. A., Kennedy, B., Knight, A., Bridges, R., Roth, K. E., Mani, E. J., Mukkadan, J. K., Nancarrow, D., Crabb, J. W., and Denton, M. J. (1997) Mutation of the gene encoding cellular retinaldehyde-binding protein in autosomal recessive retinitis pigmentosa. *Nat. Genet.* **17,** 198–200
9. Marlhens, F., Bareil, C., Griffoin, J. M., Zrenner, E., Amalric, P., Eliaou, C., Liu, S. Y., Harris, E., Redmond, T. M., Arnaud, B., Claustres, M., and Hamel, C. P. (1997) Mutations in RPE65 cause Leber's congenital amaurosis. *Nat. Genet.* **17,** 139–141
10. Marmorstein, L. Y., Munier, F. L., Arsenijevic, Y., Schorderet, D. F., McLaughlin, P. J., Chung, D., Traboulsi, E., and Marmorstein, A. D. (2002) Aberrant accumulation of EFEMP1 underlies drusen formation in malattia leventinese and age-related macular degeneration. *Proc. Natl. Acad. Sci. U.S.A.* **99,** 13067–13072
11. Stone, E. M., Lotery, A. J., Munier, F. L., Héon, E., Piguet, B., Guymer, R. H., Vandenburgh, K., Cousin, P., Nishimura, D., Swiderski, R. E., Silvestri, G., Mackey, D. A., Hageman, G. S., Bird, A. C., Sheffield, V. C., and Schorderet, D. F. (1999) A single EFEMP1 mutation associated with both malattia leventinese and Doyne honeycomb retinal dystrophy. *Nat. Genet.* **22,** 199–202
12. Weber, B. H., Vogt, G., Pruett, R. C., Stöhr, H., and Felbor, U. (1994) Mutations in the tissue inhibitor of metalloproteinases-3 (TIMP3) in patients with Sorsby's fundus dystrophy. *Nat. Genet.* **8,** 352–356
13. Suzuki, M., Tsujikawa, M., Itabe, H., Du, Z. J., Xie, P., Matsumura, N., Fu, X., Zhang, R., Sonoda, K. H., Egashira, K., Hazen, S. L., and Kamei, M. (2012) Chronic photo-oxidative stress and subsequent MCP-1 activation as causative factors for age-related macular degeneration. *J. Cell Sci.* **125,** 2407–2415
14. Yates, J. R., Sepp, T., Matharu, B. K., Khan, J. C., Thurlby, D. A., Shahid, H., Clayton, D. G., Hayward, C., Morgan, J., Wright, A. F., Armbrecht, A. M., Dhillon, B., Deary, I. J., Redmond, E., Bird, A. C., and Moore, A. T. (2007) Complement C3 variant and the risk of age-related macular degeneration. *N. Engl. J. Med.* **357,** 553–561
15. Taylor, H. R., West, S., Muñoz, B., Rosenthal, F. S., Bressler, S. B., and Bressler, N. M. (1992) The long-term effects of visible light on the eye. *Arch. Ophthalmol.* **110,** 99–104
16. Cruickshanks, K. J., Klein, R., and Klein, B. E. (1993) Sunlight and age-related macular degeneration. The Beaver Dam Eye Study. *Arch. Ophthalmol.* **111,** 514–518
17. Edwards, A. O., Ritter, R., 3rd, Abel, K. J., Manning, A., Panhuysen, C., and Farrer, L. A. (2005) Complement factor H polymorphism and age-related macular degeneration. *Science* **308,** 421–424
18. Hollyfield, J. G., Bonilha, V. L., Rayborn, M. E., Yang, X., Shadrach, K. G., Lu, L., Ufret, R. L., Salomon, R. G., and Perez, V. L. (2008) Oxidative damage-induced inflammation initiates age-related macular degeneration. *Nat. Med.* **14,** 194–198
19. Weismann, D., Hartvigsen, K., Lauer, N., Bennett, K. L., Scholl, H. P., Charbel Issa, P., Cano, M., Brandstätter, H., Tsimikas, S., Skerka, C., Superti-Furga, G., Handa, J. T., Zipfel, P. F., Witztum, J. L., and Binder, C. J.

(2011) Complement factor H binds malondialdehyde epitopes and protects from oxidative stress. *Nature* **478,** 76–81
20. Imamura, Y., Noda, S., Hashizume, K., Shinoda, K., Yamaguchi, M., Uchiyama, S., Shimizu, T., Mizushima, Y., Shirasawa, T., and Tsubota, K. (2006) Drusen, choroidal neovascularization, and retinal pigment epithelium dysfunction in SOD1-deficient mice: a model of age-related macular degeneration. *Proc. Natl. Acad. Sci. U.S.A.* **103,** 11282–11287
21. Boulton, M., and Dayhaw-Barker, P. (2001) The role of the retinal pigment epithelium: topographical variation and ageing changes. *Eye* **15,** 384–389
22. Cho, K. I., Yi, H., Tserentsoodol, N., Searle, K., and Ferreira, P. A. (2010) Neuroprotection resulting from insufficiency of RANBP2 is associated with the modulation of protein and lipid homeostasis of functionally diverse but linked pathways in response to oxidative stress. *Dis. Model. Mech.* **3,** 595–604
23. Cho, K. I., Yi, H., Yeh, A., Tserentsoodol, N., Cuadrado, L., Searle, K., Hao, Y., and Ferreira, P. A. (2009) Haploinsufficiency of RanBP2 is neuroprotective against light-elicited and age-dependent degeneration of photoreceptor neurons. *Cell Death Differ.* **16,** 287–297
24. Aslanukov, A., Bhowmick, R., Guruju, M., Oswald, J., Raz, D., Bush, R. A., Sieving, P. A., Lu, X., Bock, C. B., and Ferreira, P. A. (2006) RanBP2 modulates Cox11 and hexokinase I activities and haploinsufficiency of RanBP2 causes deficits in glucose metabolism. *PLoS Genet.* **2,** e177
25. Cho, K. I., Searle, K., Webb, M., Yi, H., and Ferreira, P. A. (2012) Ranbp2 haploinsufficiency mediates distinct cellular and biochemical phenotypes in brain and retinal dopaminergic and glia cells elicited by the Parkinsonian neurotoxin, 1-methyl-4-phenyl-1,2,3,6-tetrahydropyridine (MPTP). *Cell. Mol. Life Sci.* **69,** 3511–3527
26. Dawlaty, M. M., Malureanu, L., Jeganathan, K. B., Kao, E., Sustmann, C., Tahk, S., Shuai, K., Grosschedl, R., and van Deursen, J. M. (2008) Resolution of sister centromeres requires RanBP2-mediated SUMOylation of topoisomerase IIα. *Cell* **133,** 103–115
27. Um, J. W., Min, D. S., Rhim, H., Kim, J., Paik, S. R., and Chung, K. C. (2006) Parkin ubiquitinates and promotes the degradation of RanBP2. *J. Biol. Chem.* **281,** 3595–3603
28. Um, J. W., and Chung, K. C. (2006) Functional modulation of parkin through physical interaction with SUMO-1. *J. Neurosci. Res.* **84,** 1543–1554
29. Shimura, H., Hattori, N., Kubo, S., Mizuno, Y., Asakawa, S., Minoshima, S., Shimizu, N., Iwai, K., Chiba, T., Tanaka, K., and Suzuki, T. (2000) Familial Parkinson disease gene product, parkin, is a ubiquitin-protein ligase. *Nat. Genet.* **25,** 302–305
30. Dawson, T. M., and Dawson, V. L. (2010) The role of parkin in familial and sporadic Parkinson's disease. *Mov. Disord.* **25,** S32–S39
31. Dawson, T. M., and Dawson, V. L. (2014) Parkin plays a role in sporadic Parkinson's disease. *Neurodegener. Dis.* **13,** 69–71
32. Veeriah, S., Taylor, B. S., Meng, S., Fang, F., Yilmaz, E., Vivanco, I., Janakiraman, M., Schultz, N., Hanrahan, A. J., Pao, W., Ladanyi, M., Sander, C., Heguy, A., Holland, E. C., Paty, P. B., Mischel, P. S., Liau, L., Cloughesy, T. F., Mellinghoff, I. K., Solit, D. B., and Chan, T. A. (2010) Somatic mutations of the Parkinson's disease-associated gene PARK2 in glioblastoma and other human malignancies. *Nat. Genet.* **42,** 77–82
33. Poulogiannis, G., McIntyre, R. E., Dimitriadi, M., Apps, J. R., Wilson, C. H., Ichimura, K., Luo, F., Cantley, L. C., Wyllie, A. H., Adams, D. J., and Arends, M. J. (2010) PARK2 deletions occur frequently in sporadic colorectal cancer and accelerate adenoma development in Apc mutant mice. *Proc. Natl. Acad. Sci. U.S.A.* **107,** 15145–15150
34. Cho, K. I., Haque, M., Wang, J., Yu, M., Hao, Y., Qiu, S., Pillai, I. C., Peachey, N. S., and Ferreira, P. A. (2013) Distinct and atypical intrinsic and extrinsic cell death pathways between photoreceptor cell types upon specific ablation of Ranbp2 in cone photoreceptors. *PLoS Genet.* **9,** e1003555
35. Neilson, D. E., Adams, M. D., Orr, C. M., Schelling, D. K., Eiben, R. M., Kerr, D. S., Anderson, J., Bassuk, A. G., Bye, A. M., Childs, A. M., Clarke, A., Crow, Y. J., Di Rocco, M., Dohna-Schwake, C., Dueckers, G., Fasano, A. E., Gika, A. D., Gionnis, D., Gorman, M. P., Grattan-Smith, P. J., Hackenberg, A., Kuster, A., Lentschig, M. G., Lopez-Laso, E., Marco, E. J., Mastroyianni, S., Perrier, J., Schmitt-Mechelke, T., Servidei, S., Skardoutsou, A., Uldall, P., van der Knaap, M. S., Goglin, K. C., Tefft, D. L., Aubin, C., de Jager, P., Hafler, D., and Warman, M. L. (2009) Infection-triggered familial or recurrent cases of acute necrotizing encephalopathy caused by mutations in a component of the nuclear pore, RANBP2. *Am. J. Hum. Genet.* **84,** 44–51
36. Wolf, K., Schmitt-Mechelke, T., Kollias, S., and Curt, A. (2013) Acute necrotizing encephalopathy (ANE1): rare autosomal-dominant disorder presenting as acute transverse myelitis. *J. Neurol.* **260,** 1545–1553
37. Lönnqvist, T., Isohanni, P., Valanne, L., Olli-Lähdesmäki, T., Suomalainen, A., and Pihko, H. (2011) Dominant encephalopathy mimicking mitochondrial disease. *Neurology* **76,** 101–103
38. Ferreira, P. A., Hom, J. T., and Pak, W. L. (1995) Retina-specifically expressed novel subtypes of bovine cyclophilin. *J. Biol. Chem.* **270,** 23179–23188
39. Wu, J., Matunis, M. J., Kraemer, D., Blobel, G., and Coutavas, E. (1995) Nup358, a cytoplasmically exposed nucleoporin with peptide repeats, Ran-GTP binding sites, zinc fingers, a cyclophilin A homologous domain, and a leucine-rich region. *J. Biol. Chem.* **270,** 14209–14213
40. Yokoyama, N., Hayashi, N., Seki, T., Panté, N., Ohba, T., Nishii, K., Kuma, K., Hayashida, T., Miyata, T., and Aebi, U. (1995) A giant nucleopore protein that binds Ran/TC4. *Nature* **376,** 184–188
41. Künzler, M., Trueheart, J., Sette, C., Hurt, E., and Thorner, J. (2001) Mutations in the YRB1 gene encoding yeast ran-binding-protein-1 that impair nucleocytoplasmic transport and suppress yeast mating defects. *Genetics* **157,** 1089–1105
42. Coutavas, E., Ren, M., Oppenheim, J. D., D'Eustachio, P., and Rush, M. G. (1993) Characterization of proteins that interact with the cell-cycle regulatory protein Ran/TC4. *Nature* **366,** 585–587
43. Villa Braslavsky, C. I., Nowak, C., Görlich, D., Wittinghofer, A., and Kuhlmann, J. (2000) Different structural and kinetic requirements for the interaction of Ran with the Ran-binding domains from RanBP2 and importin-β. *Biochemistry* **39,** 11629–11639
44. Ciccarelli, F. D., von Mering, C., Suyama, M., Harrington, E. D., Izaurralde, E., and Bork, P. (2005) Complex genomic rearrangements lead to novel primate gene function. *Genome Res.* **15,** 343–351
45. Riddick, G., and Macara, I. G. (2005) A systems analysis of importin-α-β mediated nuclear protein import. *J. Cell Biol.* **168,** 1027–1038
46. Smith, A. E., Slepchenko, B. M., Schaff, J. C., Loew, L. M., and Macara, I. G. (2002) Systems analysis of Ran transport. *Science* **295,** 488–491
47. Nagai, M., Moriyama, T., Mehmood, R., Tokuhiro, K., Ikawa, M., Okabe, M., Tanaka, H., and Yoneda, Y. (2011) Mice lacking Ran binding protein 1 are viable and show male infertility. *FEBS Lett.* **585,** 791–796
48. Delphin, C., Guan, T., Melchior, F., and Gerace, L. (1997) RanGTP targets p97 to RanBP2, a filamentous protein localized at the cytoplasmic periphery of the nuclear pore complex. *Mol. Biol. Cell* **8,** 2379–2390
49. Bischoff, F. R., Krebber, H., Smirnova, E., Dong, W., and Ponstingl, H. (1995) Co-activation of RanGTPase and inhibition of GTP dissociation by Ran-GTP binding protein RanBP1. *EMBO J.* **14,** 705–715
50. Vetter, I. R., Nowak, C., Nishimoto, T., Kuhlmann, J., and Wittinghofer, A. (1999) Structure of a Ran-binding domain complexed with Ran bound to a GTP analogue: implications for nuclear transport. *Nature* **398,** 39–46
51. Izaurralde, E., Kutay, U., von Kobbe, C., Mattaj, I. W., and Görlich, D. (1997) The asymmetric distribution of the constituents of the Ran system is essential for transport into and out of the nucleus. *EMBO J.* **16,** 6535–6547
52. Kaláb, P., Pralle, A., Isacoff, E. Y., Heald, R., and Weis, K. (2006) Analysis of a RanGTP-regulated gradient in mitotic somatic cells. *Nature* **440,** 697–701
53. Carazo-Salas, R. E., Gruss, O. J., Mattaj, I. W., and Karsenti, E. (2001) Ran-GTP coordinates regulation of microtubule nucleation and dynamics during mitotic-spindle assembly. *Nat. Cell Biol.* **3,** 228–234
54. Wilde, A., Lizarraga, S. B., Zhang, L., Wiese, C., Gliksman, N. R., Walczak, C. E., and Zheng, Y. (2001) Ran stimulates spindle assembly by altering microtubule dynamics and the balance of motor activities. *Nat. Cell Biol.* **3,** 221–227
55. Clarke, P. R., and Zhang, C. (2008) Spatial and temporal coordination of mitosis by Ran GTPase. *Nat. Rev. Mol. Cell Biol.* **9,** 464–477
56. Strambio-De-Castillia, C., Niepel, M., and Rout, M. P. (2010) The nuclear pore complex: bridging nuclear transport and gene regulation. *Nat. Rev. Mol. Cell Biol.* **11,** 490–501

57. Joseph, J., Liu, S. T., Jablonski, S. A., Yen, T. J., and Dasso, M. (2004) The RanGAP1-RanBP2 complex is essential for microtubule-kinetochore interactions *in vivo*. *Curr. Biol.* **14,** 611–617
58. Salina, D., Enarson, P., Rattner, J. B., and Burke, B. (2003) Nup358 integrates nuclear envelope breakdown with kinetochore assembly. *J. Cell Biol.* **162,** 991–1001
59. Hashizume, C., Kobayashi, A., and Wong, R. W. (2013) Down-modulation of nucleoporin RanBP2/Nup358 impaired chromosomal alignment and induced mitotic catastrophe. *Cell Death Dis.* **4,** e854
60. Hamada, M., Haeger, A., Jeganathan, K. B., van Ree, J. H., Malureanu, L., Wälde, S., Joseph, J., Kehlenbach, R. H., and van Deursen, J. M. (2011) Ran-dependent docking of importin-β to RanBP2/Nup358 filaments is essential for protein import and cell viability. *J. Cell Biol.* **194,** 597–612
61. Wälde, S., Thakar, K., Hutten, S., Spillner, C., Nath, A., Rothbauer, U., Wiemann, S., and Kehlenbach, R. H. (2012) The nucleoporin Nup358/RanBP2 promotes nuclear import in a cargo- and transport receptor-specific manner. *Traffic* **13,** 218–233
62. Walther, T. C., Pickersgill, H. S., Cordes, V. C., Goldberg, M. W., Allen, T. D., Mattaj, I. W., and Fornerod, M. (2002) The cytoplasmic filaments of the nuclear pore complex are dispensable for selective nuclear protein import. *J. Cell Biol.* **158,** 63–77
63. Le, Y. Z., Zheng, W., Rao, P. C., Zheng, L., Anderson, R. E., Esumi, N., Zack, D. J., and Zhu, M. (2008) Inducible expression of cre recombinase in the retinal pigmented epithelium. *Invest. Ophthalmol. Vis. Sci.* **49,** 1248–1253
64. Cho, K. I., Patil, H., Senda, E., Wang, J., Yi, H., Qiu, S., Yoon, D., Yu, M., Orry, A., Peachey, N. S., and Ferreira, P. A. (2014) Differential loss of prolyl isomerase or chaperone activity of Ran-binding protein 2 (Ranbp2) unveils distinct physiological roles of its cyclophilin domain in proteostasis. *J. Biol. Chem.* **289,** 4600–4625
65. Yu, M., Sturgill-Short, G., Ganapathy, P., Tawfik, A., Peachey, N. S., and Smith, S. B. (2012) Age-related changes in visual function in cystathionine-β-synthase mutant mice, a model of hyperhomocysteinemia. *Exp. Eye Res.* **96,** 124–131
66. Wu, J., Peachey, N. S., and Marmorstein, A. D. (2004) Light-evoked responses of the mouse retinal pigment epithelium. *J. Neurophysiol.* **91,** 1134–1142
67. Petrukhin, K., Koisti, M. J., Bakall, B., Li, W., Xie, G., Marknell, T., Sandgren, O., Forsman, K., Holmgren, G., Andreasson, S., Vujic, M., Bergen, A. A., McGarty-Dugan, V., Figueroa, D., Austin, C. P., Metzker, M. L., Caskey, C. T., and Wadelius, C. (1998) Identification of the gene responsible for Best macular dystrophy. *Nat. Genet.* **19,** 241–247
68. Fu, S., Zhu, M., Wang, C., and Le, Y. Z. (2014) Efficient induction of productive Cre-mediated recombination in retinal pigment epithelium. *Mol. Vis.* **20,** 480–487
69. Ballestrem, C., Wehrle-Haller, B., and Imhof, B. A. (1998) Actin dynamics in living mammalian cells. *J. Cell Sci.* **111,** 1649–1658
70. Kokkinopoulos, I., Shahabi, G., Colman, A., and Jeffery, G. (2011) Mature peripheral RPE cells have an intrinsic capacity to proliferate: a potential regulatory mechanism for age-related cell loss. *PLoS One* **6,** e18921
71. Travis, G. H., Golczak, M., Moise, A. R., and Palczewski, K. (2007) Diseases caused by defects in the visual cycle: retinoids as potential therapeutic agents. *Annu. Rev. Pharmacol. Toxicol.* **47,** 469–512
72. Westenskow, P., Piccolo, S., and Fuhrmann, S. (2009) β-Catenin controls differentiation of the retinal pigment epithelium in the mouse optic cup by regulating Mitf and Otx2 expression. *Development* **136,** 2505–2510
73. Cai, H., Shin, M. C., Tezel, T. H., Kaplan, H. J., and Del Priore, L. V. (2006) Use of iris pigment epithelium to replace retinal pigment epithelium in age-related macular degeneration: a gene expression analysis. *Arch. Ophthalmol.* **124,** 1276–1285
74. van Soest, S. S., de Wit, G. M., Essing, A. H., ten Brink, J. B., Kamphuis, W., de Jong, P. T., and Bergen, A. A. (2007) Comparison of human retinal pigment epithelium gene expression in macula and periphery highlights potential topographic differences in Bruch's membrane. *Mol. Vis.* **13,** 1608–1617
75. Patel, A. K., Syeda, S., and Hackam, A. S. (2013) Signal transducer and activator of transcription 3 (STAT3) signaling in retinal pigment epithelium cells. *Jakstat* **2,** e25434
76. Chucair-Elliott, A. J., Elliott, M. H., Wang, J., Moiseyev, G. P., Ma, J. X., Politi, L. E., Rotstein, N. P., Akira, S., Uematsu, S., and Ash, J. D. (2012) Leukemia inhibitory factor coordinates the down-regulation of the visual cycle in the retina and retinal-pigmented epithelium. *J. Biol. Chem.* **287,** 24092–24102
77. Xu, K. P., and Yu, F. S. (2007) Cross talk between c-Met and epidermal growth factor receptor during retinal pigment epithelial wound healing. *Invest. Ophthalmol. Vis. Sci.* **48,** 2242–2248
78. Fuchs, U., Kivelä, T., and Tarkkanen, A. (1991) Cytoskeleton in normal and reactive human retinal pigment epithelial cells. *Invest. Ophthalmol. Vis. Sci.* **32,** 3178–3186
79. Singh, B. B., Patel, H. H., Roepman, R., Schick, D., and Ferreira, P. A. (1999) The zinc finger cluster domain of RanBP2 is a specific docking site for the nuclear export factor, exportin-1. *J. Biol. Chem.* **274,** 37370–37378
80. Yi, H., Friedman, J. L., and Ferreira, P. A. (2007) The cyclophilin-like domain of Ran-binding protein-2 modulates selectively the activity of the ubiquitin-proteasome system and protein biogenesis. *J. Biol. Chem.* **282,** 34770–34778
81. Giri, D. K., Ali-Seyed, M., Li, L. Y., Lee, D. F., Ling, P., Bartholomeusz, G., Wang, S. C., and Hung, M. C. (2005) Endosomal transport of ErbB-2: mechanism for nuclear entry of the cell surface receptor. *Mol. Cell. Biol.* **25,** 11005–11018
82. Cai, Y., Singh, B. B., Aslanukov, A., Zhao, H., and Ferreira, P. A. (2001) The docking of kinesins, KIF5B and KIF5C, to Ran-binding protein 2 (RanBP2) is mediated via a novel RanBP2 domain. *J. Biol. Chem.* **276,** 41594–41602
83. Cho, K. I., Cai, Y., Yi, H., Yeh, A., Aslanukov, A., and Ferreira, P. A. (2007) Association of the kinesin-binding domain of RanBP2 to KIF5B and KIF5C determines mitochondria localization and function. *Traffic* **8,** 1722–1735
84. Cho, K. I., Yi, H., Desai, R., Hand, A. R., Haas, A. L., and Ferreira, P. A. (2009) RANBP2 is an allosteric activator of the conventional kinesin-1 motor protein, KIF5B, in a minimal cell-free system. *EMBO Rep.* **10,** 480–486
85. Patil, H., Cho, K. I., Lee, J., Yang, Y., Orry, A., and Ferreira, P. A. (2013) Kinesin-1 and mitochondrial motility control by discrimination of structurally equivalent but distinct subdomains in Ran-GTP-binding domains of Ran-binding protein 2. *Open Biol.* **3,** 120183
86. Samuels, I. S., Sturgill, G. M., Grossman, G. H., Rayborn, M. E., Hollyfield, J. G., and Peachey, N. S. (2010) Light-evoked responses of the retinal pigment epithelium: changes accompanying photoreceptor loss in the mouse. *J. Neurophysiol.* **104,** 391–402
87. Duke-Elder, W. S., and Perkins, E. S. (1966) *Systems of Ophthalmology*, p. 675, C. V. Mosby Company, St. Louis
88. Rohrer, B., Spira, A. W., and Stell, W. K. (1993) Apomorphine blocks form-deprivation myopia in chickens by a dopamine D2-receptor mechanism acting in retina or pigmented epithelium. *Vis. Neurosci.* **10,** 447–453
89. Nagai, M., and Yoneda, Y. (2013) Downregulation of the small GTPase ras-related nuclear protein accelerates cellular ageing. *Biochim. Biophys. Acta* **1830,** 2813–2819
90. Kaylor, J. J., Yuan, Q., Cook, J., Sarfare, S., Makshanoff, J., Miu, A., Kim, A., Kim, P., Habib, S., Roybal, C. N., Xu, T., Nusinowitz, S., and Travis, G. H. (2013) Identification of DES1 as a vitamin A isomerase in Muller glial cells of the retina. *Nat. Chem. Biol.* **9,** 30–36
91. Kaneko, H., Dridi, S., Tarallo, V., Gelfand, B. D., Fowler, B. J., Cho, W. G., Kleinman, M. E., Ponicsan, S. L., Hauswirth, W. W., Chiodo, V. A., Karikó, K., Yoo, J. W., Lee, D. K., Hadziahmetovic, M., Song, Y., Misra, S., Chaudhuri, G., Buaas, F. W., Braun, R. E., Hinton, D. R., Zhang, Q., Grossniklaus, H. E., Provis, J. M., Madigan, M. C., Milam, A. H., Justice, N. L., Albuquerque, R. J., Blandford, A. D., Bogdanovich, S., Hirano, Y., Witta, J., Fuchs, E., Littman, D. R., Ambati, B. K., Rudin, C. M., Chong, M. M., Provost, P., Kugel, J. F., Goodrich, J. A., Dunaief, J. L., Baffi, J. Z., and Ambati, J. (2011) DICER1 deficit induces Alu RNA toxicity in age-related macular degeneration. *Nature* **471,** 325–330
92. Marneros, A. G. (2013) NLRP3 inflammasome blockade inhibits VEGF-A-induced age-related macular degeneration. *Cell Rep.* **4,** 945–958
93. Zhao, C., Yasumura, D., Li, X., Matthes, M., Lloyd, M., Nielsen, G., Ahern,

K., Snyder, M., Bok, D., Dunaief, J. L., LaVail, M. M., and Vollrath, D. (2011) mTOR-mediated dedifferentiation of the retinal pigment epithelium initiates photoreceptor degeneration in mice. *J. Clin. Invest.* **121,** 369–383

94. Longbottom, R., Fruttiger, M., Douglas, R. H., Martinez-Barbera, J. P., Greenwood, J., and Moss, S. E. (2009) Genetic ablation of retinal pigment epithelial cells reveals the adaptive response of the epithelium and impact on photoreceptors. *Proc. Natl. Acad. Sci. U.S.A.* **106,** 18728–18733
95. Chiang, A. C., and Massagué, J. (2008) Molecular basis of metastasis. *N. Engl. J. Med.* **359,** 2814–2823
96. Hanahan, D., and Weinberg, R. A. (2011) Hallmarks of cancer: the next generation. *Cell* **144,** 646–674